



# Hydrogeochemical and stable isotopic evidence to different water origins of karst springs in the western Himalayas, India

Rouf Ahmad Shah<sup>1</sup> · Ghulam Jeelani<sup>2</sup> · Jairam Singh Yadav<sup>1</sup> · Santosh Kumar Rai<sup>1</sup>

Received: 28 July 2021 / Accepted: 9 April 2022 / Published online: 13 May 2022  
© The Author(s), under exclusive licence to Springer-Verlag GmbH Germany, part of Springer Nature 2022

## Abstract

Karst aquifers provide tremendous benefits to the people in the Indian subcontinent, but their studies are limited due to scanty observational data. This study examines the ionic and stable isotopic composition of water samples ( $n=233$  collected between 2012 and 2014) from karst springs in the western Himalayas to determine geogenic and anthropogenic solute sources and karst aquifers recharge. A principal component analysis suggests that karst springs acquire  $\text{Ca}^{2+}$ ,  $\text{Mg}^{2+}$ ,  $\text{HCO}_3^-$ ,  $\text{Na}^+$ ,  $\text{K}^+$ , and  $\text{SO}_4^-$  through natural processes, including carbonate and silicate dissolution. With a pollution index of 38%, about 50–88% of the  $\text{NO}_3^-$ ,  $\text{F}^-$  and  $\text{Cl}^-$  contributing to karst springs have an anthropogenic origin. Karst springs are under-saturated with respect to calcite and dolomite, have higher  $\text{pCO}_2$ , and electrical conductivity is inversely related to discharge, suggesting potential of recharging waters to dissolve the host rocks along flow paths. The springs display a distinct seasonal pattern in isotope characteristics with lower values from March to May and from August to October, reflecting the recharge from the snowmelt. Occasional higher isotopic values in February, June, and July suggest episodic rainfall events. The lower values of slope ( $6.9 \pm 0.4$ ) and intercept ( $9.8 \pm 1.4$ ) along with higher  $d$ -excess ( $> 16\text{‰}$ ) of the karst springs provide strong evidence of winter snow as the primary source of recharge. Based on the karst index, the karst springs were classified as moderately to well karstified in the Liddar and Bringi catchments while slightly karstified in the Kuthar catchment. The study increases the understanding of karst aquifer sensitivity, which is necessary for implementing water supply protection schemes within the region.

**Keywords** Karst springs · Indian Himalayas · Ionic constituents · Stable water isotopes

## Introduction

Karst is a landscape where geomorphology and hydrology are largely governed by the dissolution of carbonate and/or evaporite rocks (Gutiérrez 2010; Frumkin 2013). These landscapes are greatly known for their beauty and high aesthetic value, exemplified by spectacular surface and subterranean geomorphology and complex hydrographic network (Ford and Williams 2007; Parise et al. 2018; Shah et al. 2018). They provide multiple benefits ranging from water

resources, minerals, oil, natural gas, thermal energy, tourism, and information-related paleo-environment, thus are proved crucial in promoting the regional economy (Ford and Williams 2007; Goldscheider et al. 2010; He et al. 2019). These landscapes cover 15.2% of Earth's continental surface, acting as home for 16.5% of the global population (Goldscheider et al. 2020) and supplying drinking water to nearly 10% of inhabitants around the globe (Stevanović 2019). In karst systems, groundwater and surface water coexist in a single dynamic system, where karst features provide hydraulic connections that allow an exchange of water between the surface and subsurface (Katz et al. 1997). However, these are typically challenging hydrogeological systems (Chu et al. 2017; Frumkin 2013), characterized by high heterogeneity and hydraulic anisotropy because of triple-permeability (Yu et al. 2021; Bonacci 2015; Bakalowicz 2005), which makes them highly sensitive to hydro-meteorological events (Jeelani et al. 2017a; Hartmann et al. 2014), as well as more vulnerable to geotechnical instability (Younos et al. 2019) and

✉ Rouf Ahmad Shah  
rouf@wihg.res.in

✉ Ghulam Jeelani  
geojeelani@gmail.com

<sup>1</sup> Wadia Institute of Himalayan Geology, Dehradun 248001, Uttarakhand, India

<sup>2</sup> Department of Earth Sciences, University of Kashmir, Srinagar 190006, India

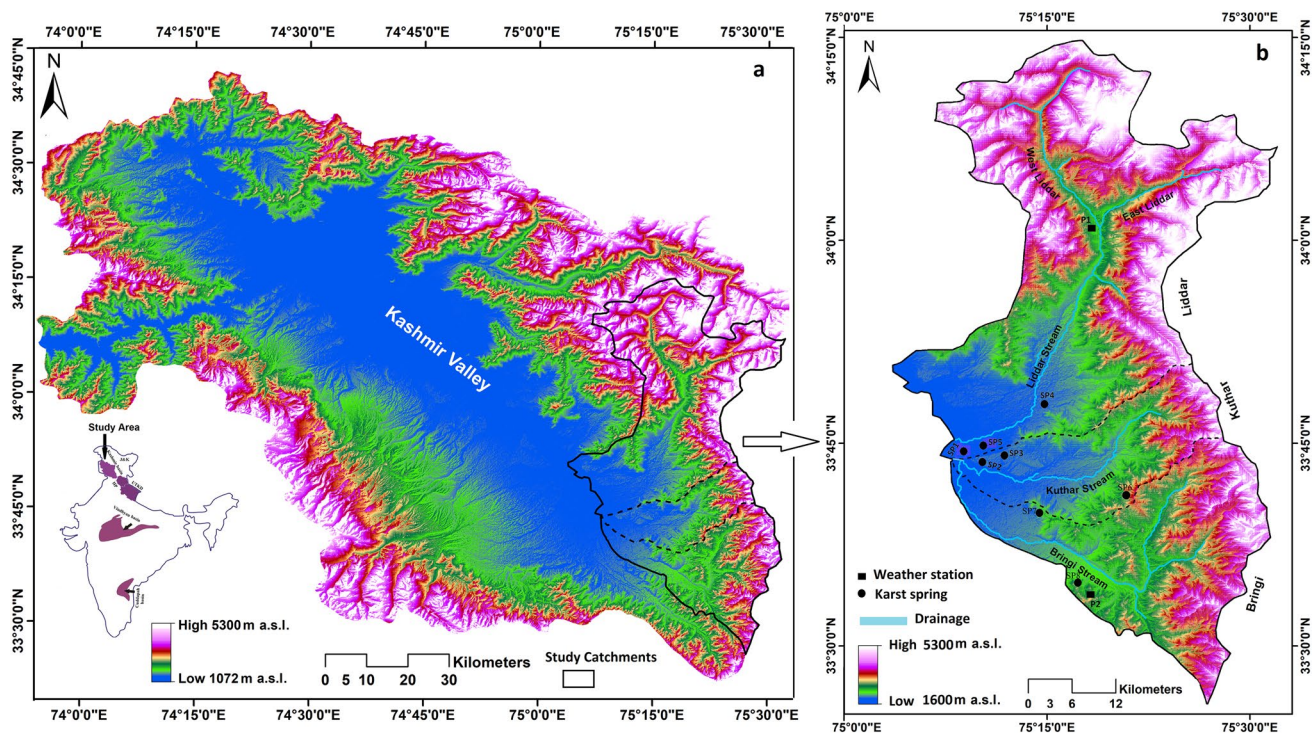


**Fig. 1** SRTM-DEM (30 m resolution) of the study area showing the location of sampling sites. Note:  $P_{1,2}$  and  $SP_{1-8}$  represent weather stations and karst springs, respectively. The SRTM-DEM was downloaded from USGS Earth Explorer

anthropogenic forcing (Chen et al. 2017; Goldscheider and Drew 2007; Perrin et al., 2004) than other aquifers (Vogelbacher et al. 2019; Ghasemizadeh et al. 2012). This presents major challenges in the theoretical and quantitative evaluation of water resources within karst basins (Stevanović 2019; Savio et al. 2019) and difficulties in defining their catchment boundaries (Gunn 2007; Parise 2016).

In India, karstified carbonate rocks are widely available and cover an area of ~8.8% (Goldscheider et al. 2020). They are largely found in the Himalayan regions such as Jammu & Kashmir (J&K), Himachal Pradesh (HP), and Uttarakhand (UTKD), where diverse surface and subsurface karst characteristics have resulted in unique landscapes (Shah et al. 2018). The karstic nature of carbonates is also apparent in other places in India (Fig. 1a; Dar et al. 2014a). They represent productive groundwater reservoirs and provide pristine drinking and irrigation water to about 35 million (even more) inhabitants in 106 districts (Dar et al. 2014a, b). Kashmir Valley, one of the largest karst regions on the Indian Subcontinent and the Indian part of the Himalayas, occupy 1100 km<sup>2</sup> (even more) of karstified carbonate rocks, of which (631 km<sup>2</sup>) lie towards its southern fringe (Shah et al. 2018); however, the karstic nature of these carbonate units is difficult to reveal at most places, because Karewa sediments typically cover them. Groundwater in these karstic rocks is the main source of clean and fresh water for about > 40% of

the local population for drinking (Jeelani 2008; Jeelani et al. 2017a), especially during summer when the demand is high for agro-horticulture and during winter when there is lean streamflow. The large karst springs are the prominent surface features of these karst landforms in the region, where few of them act as primary sources of River Jhelum (Coward et al. 1972). The development of parks and floating gardens at these spring outlets in the region labels the karst areas like state parks, featuring the region as a popular holiday destination and supporting the regional economy (Shah et al. 2018). Furthermore, the existence of some warm springs and their use for bathing and therapeutic purposes has gained more attraction (Jeelani 2004).

Despite the tremendous societal benefits, the karst aquifers in India have been least studied. Few noteworthy works by Singh (1985), Sing and Dubey (1997), and Dubey et al (2006) in the Vindhyan basin; Shibasaki et al (1985), and Dar et al (2011) in the Cuddapah basin; Jeelani (2008), Coward et al (1972), Jeelani et al (2017a; Jeelani 2008, 2011), and Shah et al (2017, 2018) in the Kashmir Basin (Fig. 1a) has highlighted some specificities of karst aquifers in some selected catchments. However, the scientific understanding and observational dataset in most of the karst regions in the Indian Himalayas are still lacking. A British team of researchers explored many Himalayan areas, particularly the Valley of Kashmir, and outlined the karst features

within carbonate rocks of the Triassic (Waltham 1972). In the Kashmir Valley, most of the recent studies (Jeelani et al. 2010, 2014, 2017a) have emphasized the delineation of groundwater catchments and recharge estimation. Only a few studies like Jeelani (2005, 2010), Jeelani et al. (2011), Bhat and Jeelani (2015), and Shah and Jeelani (2016) have evaluated the hydrochemical characteristics of groundwater and water quality indices in a few catchments. These studies considered carbonate dissolution the dominant mechanism controlling the ionic constituents in water, but this needs to be strengthened with more detailed studies.

In the study region, because of the low yield of alluvial and other porous aquifers, there is increasing stress on karst water reserves, both in flux and quality (Shah et al. 2017). At many locations within the region, the uncontrolled queries have posed a severe threat to the aquifer and the internal drainage conduits (Shah and Jeelani 2016), making groundwater more vulnerable to anthropogenic forcing. Since ionic responses in karst aquifers are more sensitive than in porous ones, updating knowledge and correct understanding of groundwater in karst aquifers is necessary for the effective management of water resources within these systems. Additionally, due to the strategic importance of karst groundwater for the entire Kashmir region, the continuous monitoring and assessment of groundwater from these karst aquifer systems have become critical. In this context, an investigation strategy was developed for assessing the groundwater in the karst aquifers of the region.

Stable water isotopes and solutes inspired a wide spectrum of interpretations of hydrological processes both at the surface and within the aquifers (Zhao et al. 2017; Jeelani et al. 2017a). Solutes (ions) in water provide meaningful insight into various geochemical processes under different flow conditions (Tang et al. 2021; Luo et al. 2018, and others), to identify the flow paths (Jeelani et al. 2014), and assess vulnerability (Shah and Jeelani 2016; Rashrash et al. 2015, and others), etc. Likewise, stable isotopes in water molecules provide the hydrological knowledge for small to large basins (Vreča and Kern 2020; Price et al. 2008). Assessment of recharge processes, estimation of residence time, mixing processes, etc., continues among the widespread benefits of stable water isotopes in hydrogeology (Shah et al. 2017; Fynn et al. 2016; McGuire et al. 2002; Clark and Fritz 1997, and others). Wang et al. (2020), Jeelani et al. (2010, 2017b) and Shah et al. (2017), and others, have used these tracers to understand the recharge processes and residence time of groundwater within karstified catchments and have achieved meaningful results. This study aims to better understand (1) the solute acquisition mechanism and flow route of groundwater using solutes and (2) to gain insights into groundwater recharge processes through stable water isotopes in three mesoscale karstified catchments of the Indian Himalayas. The desired outcome of this study will

be helpful in the implementation of drinking/irrigation water protection schemes in the karst areas and in improving the understanding of karst heterogeneity in the region.

## Study area

### Spatial extent and climate

Three representative mesoscale karstified catchments (Lid-dar, Kuthar, and Bringi) in the western Himalayas (Fig. 1) were chosen for the present study. These catchments lie between latitudes 33°16' and 34°12' N and longitudes 75°09' and 75°23' E and cover an area of ~2200 km<sup>2</sup>. The area exhibits a complex topography with an altitude ranging from 1600 to 5200 m a.s.l. The mountainous region is bestowed with abundant water reserves including glaciers, snowfields, lakes, streams, and springs. Experiencing temperate climate, the region receives an average (1964–2014) annual precipitation of 1240 mm at Pahalgam (P<sub>1</sub>: 34°01' N and 75° 19' E; at 2132 m a.s.l.), and 1010 mm at Kokernag (P<sub>2</sub>: 33°05' N and 75°18' E; at 1890 m a.s.l.) weather stations (Fig. 1b). The precipitation in the region is brought by dual monsoon systems, viz., western disturbances (> 71%), and Indian Summer Monsoons (< 29%) (Jeelani et al. 2017c). July witnesses the maximum average daily temperature (37 °C), whereas January, records the minimum average daily temperature (− 5 °C).

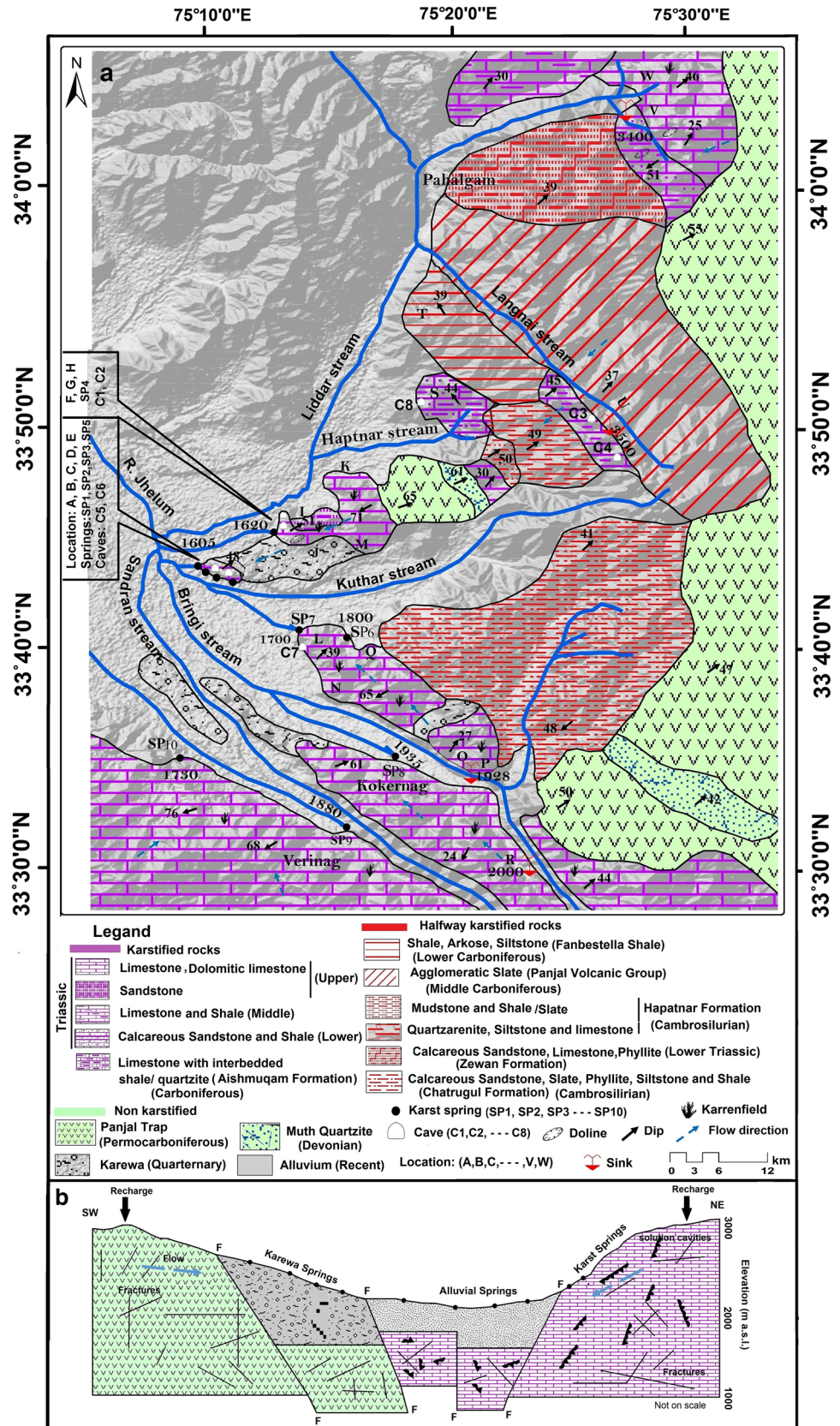
### Hydrogeology

A complex series of sedimentary formations influenced by intrusions, structural features, and erosion provides the basic hydrogeology framework in the study region. The major hydrogeological units identified are Triassic Limestone, Panjal Trap, Quaternary Karewa, and Alluvium (Fig. 2b). The Triassic Limestone is about 850 m thick and covers a large area in the study region, consisting mainly of limestone and dolomitic limestone (Middlemiss 1910; Wadia 1975). The Triassic Limestone is highly karstified and acts as a major groundwater reservoir with a hydraulic conductivity of up to 1000 m day<sup>-1</sup> (Jeelani 2007). Groundwater is discharged as perineal springs through Triassic limestone at a few to 3000 L s<sup>-1</sup> (Jeelani et al. 2018a, b). Panjal Traps consists of up to 2500 m thickness of Middle Carboniferous to Permian basaltic and andesitic rocks (Middlemiss 1910; Bhat et al. 1981), with a hydraulic conductivity of 6 m day<sup>-1</sup>, making them a productive aquifer. Many perennial springs with a flow of 20 liters per second emerge from it (Jeelani 2007).

Joints and fractures formed during periods of tectonic uplift have increased the secondary permeability in the Panjal Trap and tertiary permeability in the Triassic Limestone.



**Fig. 2 a** Karst map of the study region, depicting hydrogeological, speleological, and karst geomorphological information. Note: SP<sub>1-8</sub>, C<sub>1-8</sub> and alphabetical letters (A, B, C, – etc.) represent karst springs, caves, and local location names, respectively. **b** Map illustrating the hydrogeological framework of the study area (Jeelani 2008)





The progressive dissolution along these geological structures has played a key role in determining the flow patterns in both formations, particularly in Triassic Limestones, where extensive conduit networks are developed (Shah et al. 2018). In the studied catchments, the incision caused by tectonic upheavals and climate dominates the base-level changes of the karst extent and determines the hydrological network (Shah et al. 2018). Liddar and the Bringi catchments are among the highly karstified catchments of the region (Shah et al. 2018). Figure 2a represents the karst map of the aforementioned catchments.

Karewa covers about 5000 km<sup>2</sup>, and comprise 2000 m thick unconsolidated fluvial-glaciolacustrine sediments which include, limestones and contain sand, clay, silt, and conglomerate of Late Neogene to a Quaternary period (Datta 1983; Dar et al. 2014b). Alluvial deposits within the studied region mainly cover alluvial tracts, flood plains, and river terraces of the adjoining streams and rivers. Both Karewa and Alluvium have lower hydraulic conductivities (0.1–5 and 1–10 m day<sup>-1</sup>, respectively) because of fine sand, silt, and clay (Jeelani 2008), and the springs emerging through these have reservoirs in Triassic Limestone and Panjal Traps, respectively (Jeelani 2005). In one sense, the fault between the Triassic Limestone, the alluvium, and the Panjal Traps and Karewa provide hydraulic connection, but on the other hand, the contrasting hydraulic conductivities of the Alluvium and Karewa block groundwater flow, which leads to the existence of springs at their contact (Fig. 2b).

## Materials and methods

### Sampling

Water samples ( $n = 233$ ) were collected from karst springs in Liddar, Kuthar, and Bringi catchments in the western Himalayas from 2012 to 2014 (Fig. 1b) for hydrochemical and stable water isotope analysis. For the analysis of stable water isotopes, groundwater samples were taken fortnightly from karst springs located between 1600 and 1900 m a.s.l., in 50-mL high-density polyethylene (HDPE) bottles. While separate aliquots of filtered and unfiltered water samples were taken on a monthly basis from karst springs in 1-L HDPE bottles for ions. The samples were properly labelled and sent to respective laboratories for analysis. Additionally, hydrochemical data of one karst spring (SP<sub>8</sub>) was taken from published work (Jeelani et al. 2011).

### Analytical technique

The stable isotope ratios of oxygen and hydrogen were measured at Physical Research Laboratory (PRL) Ahmedabad, using an isotope ratio mass spectrometer (Delta V plus) in

a continuous flow mode, following the standard gas equilibration method (Maurya et al. 2009). For  $\delta^{18}\text{O}$  (or  $\delta^2\text{H}$ ) measurements, 300  $\mu\text{l}$  of water samples were equilibrated with  $\text{CO}_2$  (or  $^2\text{H}$ ) for 16 h (or 1 h), and the equilibrated  $\text{CO}_2$  (or  $^2\text{H}$ ) gas was analyzed for isotopic ratio  $^{18}\text{O}/^{16}\text{O}$  (Maurya et al. 2009). These results of the stable isotopes are reported in the standard d-notation (Coplen 1995), and defined as Vienna Standard Mean Ocean Water (VSMOW). The accuracy of measurements remains 0.1‰ for  $\delta^{18}\text{O}$  and 1‰ for  $\delta^2\text{H}$  to VSMOW. To evaluate the consistency, samples were analyzed in duplicate in each cycle of measurements.

The in situ parameters like pH, water temperature, and electric conductivity (EC) were measured by HACH (HQD Sension<sup>+</sup>), whereas major ion ( $\text{Ca}^{2+}$ ,  $\text{Mg}^{2+}$ ,  $\text{Na}^+$ ,  $\text{K}^+$ ,  $\text{Fe}^{2+}$ ,  $\text{HCO}_3^-$ ,  $\text{Cl}^-$ ,  $\text{NO}_3^-$ ,  $\text{F}^-$ ) analysis was carried out at Hydrogeology Laboratory, Department of Earth Sciences, University of Kashmir. Standard methods were adopted to analyze the dissolved chemical constituents (APHA, 2001).  $\text{Ca}^{2+}$ ,  $\text{Mg}^{2+}$  was analysed by EDTA titration;  $\text{HCO}_3^-$  was measured by HCl titration;  $\text{Cl}^-$  by  $\text{AgNO}_3$  titration;  $\text{Na}^+$  and  $\text{K}^+$  by flame emission photometry;  $\text{SO}_4^-$  and  $\text{NO}_3^-$  by spectrophotometer; and  $\text{Fe}^{2+}$  and  $\text{F}^-$  by the Colorimeter. During the analytical procedures, blanks and standards were run to check the methods' reliability. Analytical precision was within  $\pm 6\%$  for major ions.

### Principal component analysis

To evaluate the factors regulating the water chemistry, the effect of host rock lithology on water chemistry principal component analysis (PCA) of hydrochemical data was performed using XLSTAT software ([www.xlstat.com](http://www.xlstat.com)). The PCA is a useful tool to identify the processes contributing the groundwater chemistry and quality (Zakhem et al. 2017; Wu et al. 2014, 2020). It reduces a large data matrix to a new matrix with fewer dimensions (Liu et al. 2020; Li et al. 2019). In the present study, the hydrochemical data (Table 1) of the karst springs were standardized and subjected to the PCA to characterize the processes controlling the solute mechanism.

In the PCA, the similarity matrix (Eq. 1) was used to generate eigenvalues and scores for the data series. The significant principal components (PCs) were determined using the eigenvalue > 1 rule (Kaiser 1960) and Scree test (Cattell 1966). Based on scree classification, three principal components  $F_1$ ,  $F_2$ , and  $F_3$ , with eigenvalues > 1, were chosen to assess the factor loading and various variables (Ren et al. 2021). Accordingly, the first three principal components (PCs), accounting for the majority of the variation (> 60%), were used for interpretation, while the  $F_1$  and  $F_2$  components were considered for bi-plots. Earlier studies (Lee et al. 2003) have proposed

**Table 1** The statistical summary including arithmetic means, minimum, maximum and standard deviation of ionic constituents of karst springs

Karst Springs	Catchment	ID	Para-meter	pH	Water temp (°C)	EC ( $\mu\text{s cm}^{-1}$ )	Ca <sup>2+</sup>	Mg <sup>2+</sup>	Na <sup>+</sup>	K <sup>+</sup>	Fe <sup>2+</sup>	Cl <sup>-</sup>	HCO <sub>3</sub> <sup>-</sup>	SO <sub>4</sub> <sup>-</sup>	NO <sub>3</sub> <sup>-</sup>	F <sup>-</sup>	Saturation index	
																	Calcite	Dolomite
Andernag	Liddar	SP <sub>1</sub>	Min	6.9	10	392	87	49.1	20	3.1	22.2	24.5	487	3.0	2.2	0.6	-0.3 to 0.95	-0.6 to 1.62
			Max	8.5	14	469	105	63.7	27.8	5.3	33.2	33.4	550	5.3	3.4	1.3		
			Avg	7.8	12.2	434	97	55.2	24.2	4	28.1	27.7	513	4	2.8	0.9		
			S.D.	0.4	1.4	25.5	5.5	4.8	2.3	0.7	4	2.5	22	0.7	0.4	0.2		
Malakhmag	Kuthar	SP <sub>2</sub>	Min	7.3	17.3	319	68	36.9	24	7.1	1.3	17.1	457	11	3.1	0.6	-0.1 to 0.61	-0.2 to 1.26
			Max	9.1	22	455	98	60.4	36	12.2	3.3	21.1	500	17.3	5.6	1.8		
			Avg	8.0	19.5	355	87	48.1	29.8	9.7	2.2	19.3	479	14.4	4.5	1.0		
			S.D.	0.5	1.6	37.7	9.1	7.6	3.7	1.7	0.6	1.4	14.1	1.9	0.7	0.3		
Sayednag	Kuthar	SP <sub>3</sub>	Min	7.5	17	299	54	30.8	20.2	2.4	2.2	11.3	285	42	2.9	0.7	-1 to 0.98	-2 to 1.91
			Max	8.7	20	448	65	37	28.6	6.6	5.8	20.8	327	63.0	5.2	2		
			Avg	7.9	17.2	388.6	59	33.7	24	4.7	3.8	16.4	313	52.3	4.2	1.2		
			S.D.	0.4	1.7	39.4	3.3	2	2.7	1.2	1.2	2.8	12.2	6.5	0.6	0.2		
Martandnag	Liddar	SP <sub>4</sub>	Min	7.2	11.1	298	74	36.3	10.1	2.4	10.8	11	470	2.9	1.3	0.5	-0.8 to 0.98	-1.6 to 1.85
			Max	8.6	16.7	375	101	54.8	30.1	6.2	19.7	16.6	496	7.8	4.6	1.1		
			Avg	8.0	14	332.5	93	48.4	20.3	4.6	15.2	13.8	485	4.6	2.6	0.9		
			S.D.	0.4	2.3	21.4	9	5.7	5.3	1.1	2.5	2.1	8.8	1.6	0.9	0.1		
Gujjang	Liddar	SP <sub>5</sub>	Min	7.2	12	328	70	38.2	21	7.2	16.1	15.3	408	3	1.7	0.9	0.3 to 0.73	-0.5 to 2.12
			Max	9.4	16	473	84	49.3	35	11.8	19.6	24	489	5.2	3.2	1.2		
			Avg	8.0	14.3	381.1	79	43.1	28.4	9.8	17.7	17.7	430.9	4.2	2.4	0.8		
			S.D.	0.8	1.2	46.9	3.8	3.7	3.9	1.6	1	2.6	26.9	0.8	0.5	0.4		
Daidnag	Bringi	SP <sub>6</sub>	Min	7.8	11	283.0	55	33.6	20	5.1	1.5	8.9	327	12.1	1.1	0.7	-1.1 to 1.09	-2 to 2.10
			Max	9.4	17.3	386.0	100	55.7	34	10.3	5.2	19.6	512	42	5.1	1.5		
			Avg	8.3	13	347.9	83	45.3	25.1	7.8	2.8	15.1	451.1	21.8	3.1	1.1		
			S.D.	0.5	2	40.3	18.4	8.7	4.8	1.9	1.5	3.5	77	12.3	1.3	0.3		
Achabalanag	Bringi	SP <sub>7</sub>	Min	7.1	12.8	309.0	81.2	40.2	11	2	1	9.3	456.4	9.4	2.3	0.4	-1.7 to 0.94	-3 to 1.79
			Max	9.4	16	376.0	100	58.2	34	10.3	3.2	21.1	525.0	16.4	5.1	1.3		
			Avg	8.2	13.7	338.4	92	48.6	20.1	5.8	2.1	15.9	495.7	14.5	3.8	0.9		
			S.D.	0.7	1	23.4	6.5	5.6	8.2	2.9	0.6	3.7	22.8	1.9	0.9	0.2		
Kokernag	Bringi	SP <sub>8</sub>	Min	7.1	12.6	283.0	55	34	17	2	1.7	10	303	9	1.1	0.3	-1.5 to 0.97	-1.7 to 2.18
			Max	9.4	16.3	468.0	96	76	34	11.8	3.2	22.0	532	27	5.1	1.2		
			Avg	7.9	14.2	345.8	83	48.5	22.8	5.9	2.2	16.5	425.7	15	3	0.78		
			S.D.	0.7	1.3	47.2	14.5	11.1	5.3	3.3	0.6	3.4	80	5.8	1	0.4		

the factor loading classification into strong (>0.75), moderate (0.75–0.5), and weak classes (<0.5), respectively.

$$F_{jk} = a_{j1}x_{k1} + \dots + \dots a_{jn}x_{kn} \tag{1}$$

$F_{jk}$  represents the principal component value for object  $j$  on component  $k$ ,  $a_{jl}$  is the loading of element  $l$  on component  $j$ ,  $x_{kl}$  is the length of the score for variable  $l$  on item  $k$ , and  $n$  represents the entire amount of observed variables.

The saturation index (SI) of minerals was calculated using the PHREEQC geochemical software (Parkhurst and Appelo 2013) by comparing the chemical activities of dissolved ions in view of minerals (ion activity product, IAP) with their solubility product ( $K_{sp}$ ). In the present study, considering the presence of  $Cl^-$ ,  $NO_3^-$ , and  $F^-$  concentrations in spring waters due to anthropogenic forcing, the pollution index was calculated (Vinnarasi et al. 2021) using the below formula (in  $\mu eq L^{-1}$ ).

$$\left\{ \frac{(Cl^- + NO_3^-)}{(Cl^- + NO_3^- + F^-)} \right\} \times 100 \tag{2}$$

To classify the studied karst spring and provide meaningful insights on the subsurface heterogeneity, ionic/isotopic and hydrologic parameters of low and high flow rates were linked to each other to evaluate the karst index below. Various researchers across the globe have validated the index to classify the springs (Atkinson 1977; López-Chicano et al. 2001; Vesper and White 2003; Heinz et al. 2009; Mustafa and Merkel 2015).

$$k_i = M \times 100 \tag{3}$$

$$M = \sum_{i=1}^n k_i / n \tag{4}$$

$$k_i = \frac{Q_{\text{minimum}} \times iQ_{\text{minimum}}}{Q_{\text{maximum}} \times iQ_{\text{maximum}}} \tag{5}$$

where  $M$  is the arithmetic mean and  $k_i$  represents the ratio of flow ( $Q$ ) multiplied by their corresponding values for a specific ionic/isotopic parameter ( $i$ ) of a spring under low and high flow periods, and  $n$  is the number of constituents/parameters. To understand the seasonal variation of solutes in the karst springs, a mass balance equation was used to estimate the dilution factor (Absar et al. 1991) with the assumption that  $X$  fraction of diluting water mixed  $1-X$  pre-event (lean flow) water fraction to produce post-event (high flow) diluted water.

## Results

### Ionic composition of groundwater

The observed variation in the ionic constituents of the karst springs during the monitoring period is summarized in terms of minimum, maximum, mean, and standard deviation in Table 1. The spring water is alkaline in nature, with a pH ranging from 6.9 to 9.4. Water temperatures vary from 10 to 22 °C with springs (SP<sub>2</sub> and SP<sub>3</sub>) in Liddar (SP<sub>1</sub>, SP<sub>4</sub>, SP<sub>5</sub>) and Bringi (SP<sub>6</sub>, SP<sub>7</sub>, SP<sub>8</sub>) catchments attaining temperatures below 17 °C, while springs in Kuthar (SP<sub>2</sub>, SP<sub>3</sub>) achieved higher temperatures over 17 °C. The PCA results showed maximum positive loading (0.90 and 0.87) for Ca<sup>2+</sup> and Mg<sup>2+</sup> followed by HCO<sub>3</sub><sup>-</sup> (0.82) and Cl<sup>-</sup> (0.81) in the Liddar catchment. In the Kuthar catchment, the highest positive loading was found for HCO<sub>3</sub><sup>-</sup> (0.95) followed by K<sup>+</sup> (0.91) and Ca<sup>2+</sup> (0.90). However, in the Bringi catchment, Ca<sup>2+</sup> (0.77) followed by HCO<sub>3</sub><sup>-</sup> (0.64) contributes to the spring waters' major proportion. The strong positive factor loading (except Cl<sup>-</sup> which shows moderate loading) on Na<sup>+</sup>, Ca<sup>2+</sup>, Mg<sup>2+</sup>, K<sup>+</sup>, and HCO<sub>3</sub><sup>-</sup> with a variance of 51.65% is witnessed in the spring water ionic constituents in the Kuthar catchment with respect to the  $F_1$  component (Fig. 3). Similarly, strong positive loading on EC, SO<sub>4</sub><sup>-</sup>, Cl<sup>-</sup>, HCO<sub>3</sub><sup>-</sup>, Ca<sup>2+</sup> and Mg<sup>2+</sup> was seen in the Liddar catchment with a variance of 40.30% in the ionic constituents (Fig. 2). In contrast, the springs in the Bringi catchment displayed 36.08% variance with moderate to strong positive factor loading on HCO<sub>3</sub><sup>-</sup>, Ca<sup>2+</sup>, and Mg<sup>2+</sup> with respect to the  $F_1$  component (Fig. 3). The  $F_2$  component accounts for 23.81% and 16.02% of the total variance in the Liddar and the Kuthar catchments (Fig. 3), with negative loading on NO<sub>3</sub><sup>-</sup>, EC, K<sup>+</sup>, Cl<sup>-</sup>, F<sup>-</sup>, and weak negative loading on the rest of the ionic constituents, respectively. While the  $F_2$  component in the Bringi catchment (Fig. 3) exhibited a 24.47% variance in ionic constituents with strong positive loading on K and moderate on Ca<sup>2+</sup>, Na<sup>+</sup>, HCO<sub>3</sub><sup>-</sup>. There is positive loading on EC, Cl<sup>-</sup>, Mg<sup>2+</sup>, NO<sub>3</sub><sup>-</sup>. Furthermore, there is strong positive loading on EC, Ca<sup>2+</sup>, Mg<sup>2+</sup>, Na<sup>+</sup>, K<sup>+</sup>, HCO<sub>3</sub><sup>-</sup> and weak negative loading on others with respect to  $F_3$  (Table 2), accounting for 10.75% variance in ionic constituents in the Kuthar catchment. This variance is higher (12.8% with respect to  $F_3$ ) in the Bringi catchments with most of the negative loading except Mg<sup>2+</sup>, Cl<sup>-</sup>, NO<sub>3</sub><sup>-</sup>, and F<sup>-</sup>. The springs in the Liddar catchment displayed intermediate variance (10.74%) with negative loading on EC, K<sup>2+</sup>, and Fe<sup>2+</sup> and weak positive loadings on other ions. It is observed that  $F_1$  and  $F_2$  components mainly control the ionic composition of the karst spring in the studied region; therefore, principal components ( $F_4$ ... $F_{12}$ ) have a lower variance (<8%) and were not considered (Fig. 3).



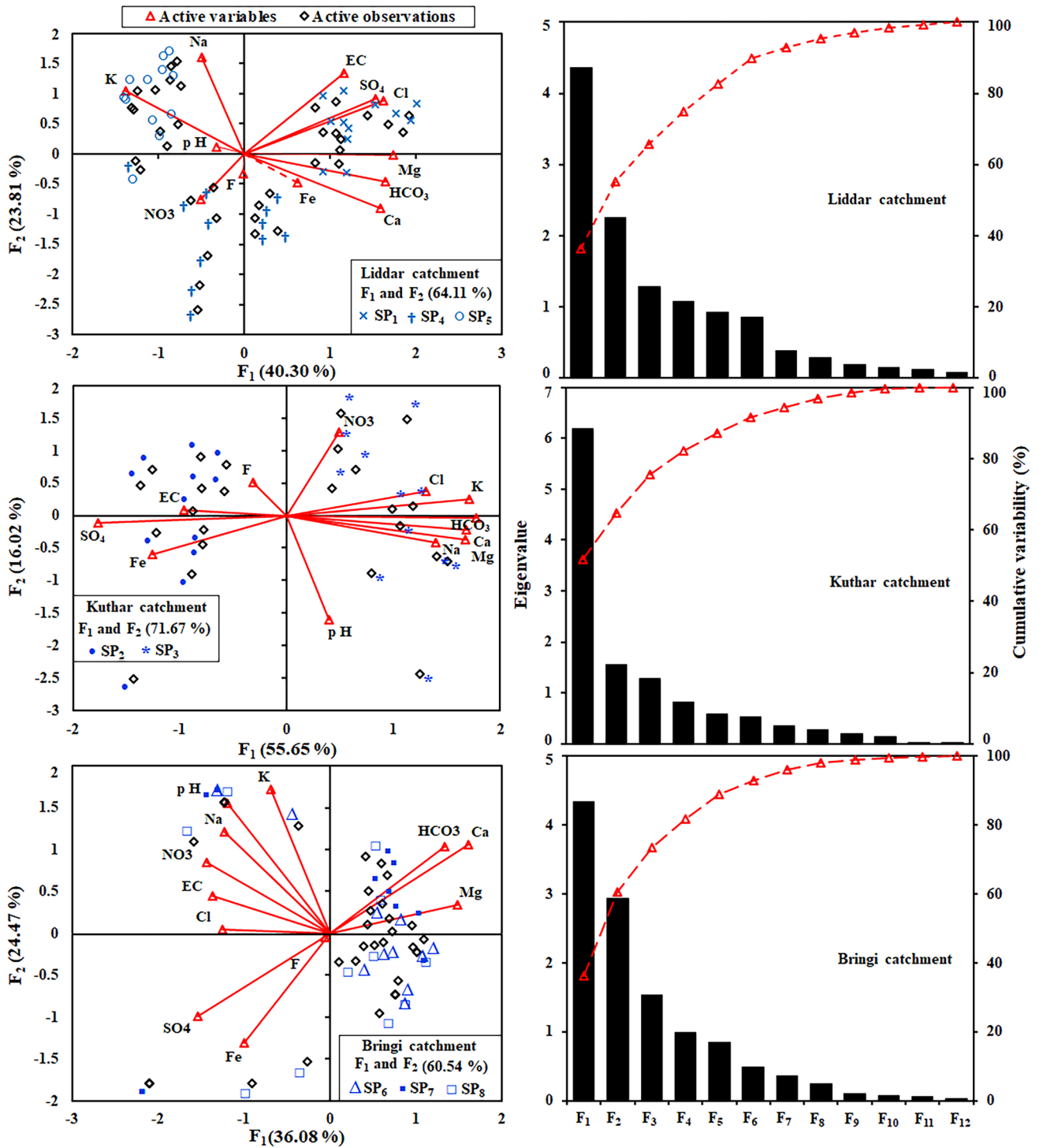


Fig. 3 Principal component analysis of karst springs showing the ionic variability and controlling factors

The saturation index (SI) results indicate that karst springs in each catchment are under-saturated with calcite and dolomite (refer to Table 1). Furthermore, it is observed that computed partial pressure pCO<sub>2</sub> for the karst springs is slightly higher (10<sup>-3</sup> × 4.1) to (10<sup>-1</sup> × 2.5) than

the atmospheric level (10<sup>-3.5</sup>). The results also show that solutes (here EC) exhibit a similar pattern in all the karst springs, a seasonality based on the flow patterns (Fig. 4), with dilution factors ranging from 27 to 53% in higher flow conditions.

**Table 2** Factor loadings of principal components ( $F_1$  to  $F_4$ ) of Karst springs in Bringi, Kuthar, and Liddar catchments

Parameters	Bringi				Kuthar				Liddar			
	$F_1$	$F_2$	$F_3$	$F_4$	$F_1$	$F_2$	$F_3$	$F_4$	$F_1$	$F_2$	$F_3$	$F_4$
pH	-0.57	0.75	-0.15	-0.04	0.22	-0.86	-0.15	-0.01	-0.16	0.06	0.65	0.08
EC	-0.66	0.21	0.00	0.51	-0.52	0.05	0.34	0.75	0.58	0.67	-0.05	0.16
Ca <sup>2+</sup>	0.77	0.51	-0.03	-0.01	0.90	-0.12	0.25	-0.02	0.79	-0.45	0.09	0.05
Mg <sup>2+</sup>	0.71	0.17	0.06	0.59	0.90	-0.20	0.06	-0.06	0.87	-0.01	0.05	-0.29
Na <sup>+</sup>	-0.59	0.58	-0.01	0.10	0.75	-0.22	0.01	0.28	-0.25	0.80	0.22	-0.01
K <sup>+</sup>	-0.33	0.82	-0.32	-0.07	0.92	0.14	0.01	-0.11	-0.69	0.52	-0.04	0.07
Cl <sup>-</sup>	-0.60	0.02	0.51	-0.48	0.70	0.20	-0.25	0.10	0.81	0.44	0.07	0.13
HCO <sub>3</sub> <sup>-</sup>	0.64	0.50	-0.03	-0.30	0.95	-0.02	0.16	0.03	0.82	-0.23	0.10	-0.27
SO <sub>4</sub> <sup>-</sup>	-0.74	-0.47	-0.35	0.02	-0.95	-0.06	-0.08	-0.07	0.76	0.46	0.16	0.26
NO <sub>3</sub> <sup>-</sup>	-0.69	0.40	0.31	0.12	0.26	0.69	-0.52	0.02	-0.25	-0.38	0.44	0.53
Fe <sup>2+</sup>	-0.48	-0.63	-0.20	0.08	-0.68	-0.33	-0.20	-0.20	0.31	-0.24	-0.33	0.72
F <sup>-</sup>	-0.03	-0.02	0.94	0.17	-0.17	0.28	0.83	-0.31	-0.01	-0.16	0.68	-0.07

### Stable water isotopes in karst springs

In the study region, karst springs showed wide variability in  $\delta^{18}\text{O}$  and  $\delta^2\text{H}$  ( $\delta$ -values) at spatial and temporal scales (Table 3, Fig. 5). The  $\delta^{18}\text{O}$  values range from  $-6.3$  to  $-10.4\text{‰}$  while the  $\delta^2\text{H}$  values range from  $-58$  to  $-38.3\text{‰}$ . A similar temporal pattern with no major shift in isotopic (or  $\delta$ ) characteristics of all the karst springs was observed (Fig. 5). Enriched isotopic values were observed in each catchment during the summer months, while depleted values were reported during the spring and autumn months. However, subtle differences in  $\delta^{18}\text{O}$  and  $\delta^2\text{H}$  of karst springs were noticed on a spatial scale (Fig. 5). It was observed that  $\delta$ -values of karst springs do not vary as a function of altitude. Overall, statistically, there exists an insignificant correlation ( $R^2$ : 0.11,  $p$ : 0.06) between the altitude of karst springs and their  $\delta$ -values.

The d-excess ( $d$ ) also vary substantially, from 7.3 to 32.7‰ with an average of 19‰ (Table 3, Fig. 6a). Though there is a small spatial variation in the  $d$  of the karst springs, a distinct temporal pattern in isotope characteristics of the karst springs was observed in all the catchments (Fig. 6a). The  $d$  varied from 7.3 to 31‰ in the Liddar, 10.7–23.6‰ in the Bringi, and 8.4–32.7‰ in the Kuthar catchments. Overall, nearly 75% of groundwater samples showed  $d > 16\text{‰}$ , complementing its close link to winter precipitation. Jeelani et al. (2017c) reported that winter precipitation across the western Himalayas exhibits higher  $d$  ( $> 15\text{‰}$ ). The  $\delta^{18}\text{O}$  versus  $\delta^2\text{H}$  regression plot (Fig. 6c) of all the karst springs showed a lower slope and lower intercept (collective:  $6.9 (\pm 0.4) \times \delta^{18}\text{O} + 9.7 (\pm 1.4)$ ;  $R^2 = 0.85$ ) compared to the global meteoric water line (GMWL) and the reported local meteoric water line (LMWL: by Jeelani et al. 2017c, 2018a). Despite a slight variance noted in their slopes (Liddar:  $5.4 \pm 0.11$ , Kuthar:  $5.2 \pm 0.21$ , and Bringi:  $5 \pm 0.17$ ) and

intercepts of the groundwater regression lines at a catchment level (Liddar:  $10 \pm 0.4$ , Kuthar:  $7.8 \pm 1.2$ , and Bringi:  $9.8 \pm 1$ ), their relation with these two meteoric water lines shows that samples are overlapped and closely approached (Fig. 6b). The results further reveal that springs in the Liddar and Bringi catchments have higher amplitudes (1.9–3 and 1.5–3.3, respectively, for  $\delta^{18}\text{O}$ ), close to precipitation (4–5.6) in those catchments. However, the springs in the Kuthar catchment have a lower amplitude (0.9–1.8), than precipitation in the catchment.

## Discussion

### Solute source and flow routes

Variance observed between the chemical parameters as the highest loading factors is usually used to identify the geochemical processes involved (Rao et al. 2007; Zakhem et al. 2017). In the study region, the higher positive loading on Ca<sup>2+</sup>, Mg<sup>2+</sup>, and HCO<sub>3</sub><sup>-</sup> with respect to the  $F_1$  component evinces the natural mineralization and/or dissolution of hosted carbonate rocks (refer, Fig. 3, Li et al. 2016, 2018). Their studies (Bhat and Jeelani 2015) and Shah and Jeelani (2016) reported that carbonate weathering mainly contributes to the region's Ca<sup>2+</sup>, Mg<sup>2+</sup>, and HCO<sub>3</sub><sup>-</sup> to groundwater. While moderate-to-weak loading on NO<sub>3</sub><sup>-</sup>, Cl<sup>-</sup>, and F<sup>-</sup>, accounting for the 16–24% variance for  $F_2$ , indicates the anthropogenic input (e.g., Esteller and Andreu 2005). Considering the geology of the studied region and the ionic analysis, the positive loading such as Ca<sup>2+</sup>, Mg<sup>2+</sup>, and HCO<sub>3</sub><sup>-</sup> represent the natural processes by which spring water acquires its chemical signatures (e.g., Nesrine et al. 2015), whereas moderate-to-weak loadings on ionic concentrations such as NO<sub>3</sub><sup>-</sup>, Cl<sup>-</sup> and F<sup>-</sup> represents

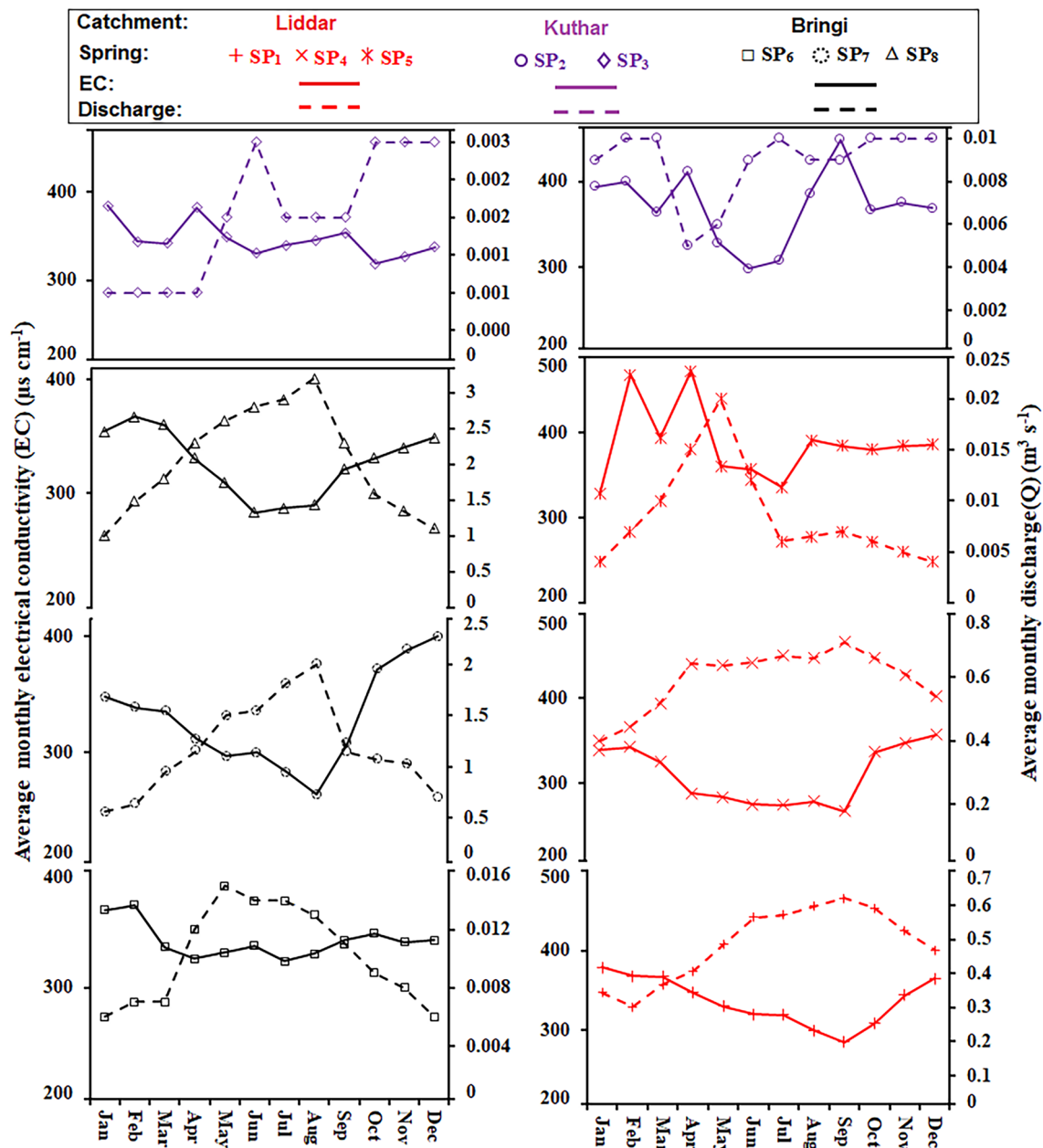


**Fig. 4** Relationship between electrical conductivity (EC) and discharge (Q) of karst springs in the study region

anthropogenic forcing (Esteller and Andreu 2005; Dragon and Gorski 2015). Earlier studies (e.g., Shah et al. 2017; Bhat and Jeelani 2015; Jeelani et al. 2011; Jeelani 2010) have demonstrated the anthropogenic origin of these solutes in waters of the studied region. The anthropogenic contribution to  $\text{NO}_3^-$  and  $\text{Cl}^-$  is evident from the higher  $\text{NO}_3^-/\text{Na}^+$  and  $\text{Cl}^-/\text{Na}^+$  ratios (Fig. 7a), where some data points are shifted towards right above a 1:1 equiline. The  $\text{NO}_3^-/\text{Na}^+$  and  $\text{Cl}^-/\text{Na}^+$  ratios are usually used to quantify the anthropogenic input (Kou et al. 2019). This study (based on Eq. 2 and Fig. 7a) suggests that anthropogenic

forcing contributes to about 38% of pollution in these catchments, including 1–38% in the Bringi, 9–24% in the Kuthar, and 2–31% in the Liddar. Therefore, 50–88% of  $\text{NO}_3^-$ ,  $\text{F}^-$ , and  $\text{Cl}^-$  ions contributed to karst springs are derived from anthropogenic forcing. Overuse of pesticides and fertilizers to horticultural plantations on karst ridges affects the water table through sensitive features on the surface (Shah and Jeelani 2016). In addition, the depressions/sinks along stream banks used for dumping (particularly in the Bringi catchment, where numerous vertical shafts and sinkholes have been found along the Bringi stream at places such as



**Table 3** The statistical summary including arithmetic means, minimum, maximum, and standard deviation of  $\delta^{18}\text{O}$  and  $\delta^2\text{H}$  and the d-excess (*d*) in the karst springs

Karst springs	Catchment	ID	Altitude (m, a.s.l.)	$\delta^{18}\text{O}(\text{‰})$					$\delta^2\text{H}(\text{‰})$					D-excess ( $\text{‰}$ )		
				Min	Max	Mean	W.M	S.D.	Min	Max	Mean	W.M	S.D.	Min	Max	Mean
Andernag	Liddar	SP <sub>1</sub>	1609	-9.1	-7	-7.9	-5.4	0.7	-54.8	-38.6	-47.4	-32.1	5.0	10	26	17
Malakhnag	Kuthar	SP <sub>2</sub>	1616	-9.5	-8.7	-8.6	-6.8	0.9	-55.1	-46.4	-50.2	-36	5.2	11.4	32.7	18
Sayeednag	Kuthar	SP <sub>3</sub>	1611	-9.6	-7.8	-8.8	-3.4	0.5	-56.8	-46.4	-57.6	-29	4.1	8.4	30	21
Martandnag	Liddar	SP <sub>4</sub>	1680	-10.4	-7.4	-8.5	-5.6	0.8	-59	-43.1	-50.7	-31	5.1	7.4	31	18
Gujnag	Liddar	SP <sub>5</sub>	1613	-9.6	-7.7	-9.1	-7.1	0.6	-57.6	-43.9	-54.4	-38.3	5.0	12.4	22	20
Daidnag	Bringi	SP <sub>6</sub>	1750	-10	-7.2	-8.3	-4.3	1.0	-55.5	-42.7	-50.2	-30	5.6	10.7	18.7	17
Achabalnag	Bringi	SP <sub>7</sub>	1702	-9.6	-6.3	-7.9	-4	0.8	-55.3	-38.4	-46.6	-25	6.2	11.4	23.6	19
Kokernag	Bringi	SP <sub>8</sub>	1890	-8.8	-7.3	-8.1	-4.7	0.6	-50.2	-41.3	-47	-29	3.2	16	20	18

Adigam, Dewalgam, Gadol, Wandevalg, etc.) remain underwater during periods of high flow, adding toxicity to the flow (Shah and Jeelani 2016; Jeelani et al. 2018b). Rasool et al. (2021) found an increasing trend in both horticultural and built-up practices throughout the last 30 years in some catchments, including that under study (Fig. 7b). Similarly, the strong positive loading of EC,  $\text{Ca}^{2+}$ ,  $\text{Mg}^{2+}$ ,  $\text{Na}^+$ ,  $\text{K}^+$ ,  $\text{HCO}_3^-$  with respect to  $F_3$ , accounting for 10.75–12.8% of the variance in solutes, also suggests that geogenic processes are determining the chemistry of spring water. The geogenic sources of these solutes in the catchment waters have also been reported (e.g. Jeelani et al. 2011).

To further assess the geogenic factors controlling the spring water chemistry, hydrochemical data were plotted as,  $\text{Ca}^{2+} + \text{Mg}^{2+}$  versus  $\text{HCO}_3^- + \text{SO}_4^-$  (Fig. 8a), where most of the data points fall above the aquiline. This suggests the significant contribution of carbonate and silicate dissolution in contributing to the ionic composition of the karst springs (Li et al. 2016, 2018; Wei et al. 2021). Since the proportion of  $\text{Ca}^{2+}$  and  $\text{Mg}^{2+}$  to the groundwater environment is mainly by carbonate lithologies within the study region, the  $\text{Mg}^{2+}/\text{Ca}^{2+}$  molar ratios are used to estimate the calcite and dolomite weathering input (Szramek et al. 2011; Shah and Jeelani 2016). The calculated values (0.09–1.1) reveal that spring water in the studied region exhibit a wide range and shows dominance of calcite dissolution (77% of samples) over dolomite dissolution (33% of samples). In  $\text{Ca}^{2+} + \text{Mg}^{2+} - \text{HCO}_3^- - \text{SO}_4^-$  versus  $\text{Na}^+ - \text{Cl}^-$  plot (Fig. 8c), most data points are scattered patterns. However, they lie close to equiline with a slope of ~80% towards the positive trend, confirming that  $\text{Ca}^{2+}$ ,  $\text{Mg}^{2+}$ , and  $\text{Na}^+$  are interrelated through ion exchange during carbonate and silicate weathering. The role of silicate weathering is further supported by the  $\text{Na}^+ + \text{K}^+/\text{TZ}^+$  ratio (Fig. 8b), ranging between 0.4 and 1.3. The values clearly infer the release of Na and K to the groundwater environment from silicate rocks (Das and Kaur 2001).

Characterisation of  $\text{Ca}^{2+} - \text{HCO}_3^-$  and  $\text{Ca}^{2+} - \text{Mg}^{2+} - \text{HCO}_3^-$  water types evinces that major ionic constituents in the spring waters show dominance of alkaline earth water group over the alkalis (refer, Fig. 9, 8d, 10). The  $\text{Ca}^{2+} - \text{HCO}_3^-$  and  $\text{Ca}^{2+} - \text{Mg}^{2+} - \text{HCO}_3^-$  water types indicate young recharging water (Ophori and Toth 1989). A similar facies pattern ( $\text{Ca}^{2+} - \text{HCO}_3^-$ ) in all the karst springs within the Bringi basin (refer, Fig. 9). However, more than one water type ( $\text{Ca}^{2+} - \text{HCO}_3^-$  and  $\text{Ca}^{2+} - \text{Mg}^{2+} - \text{HCO}_3^-$ ) in springs of Liddar and Kuthar catchments reveals preferential flow through multiple lithologies such as carbonates and silicates. The increasing concentration of  $\text{F}^-$  and  $\text{HCO}_3^-$  in the karst springs with a downward direction from SP<sub>8</sub> to SP<sub>6</sub> in the Bringi, SP<sub>4</sub> to SP<sub>1</sub> in the Liddar, and from SP<sub>3</sub> to SP<sub>2</sub> in the Kuthar catchment (refer, Table 1, Fig. 8e), suggest the direction of the flow pattern/or recharging waters with each catchment. The inverse relationship between discharge and electrical conductivity (Fig. 4), and the dilution factor of 26–53%, suggest that new and relatively dilute water is being added to the aquifer in the spring and early summer seasons, hence causing strong dilution effects on the groundwater chemistry in each catchment. When the temperature increases, the increasing discharge associated with decreasing EC from March onwards (Fig. 4) validates the simultaneous addition of melt-water released from winter accumulated snowpacks to the aquifers. In contrast, the increase of EC from August/September to October results from higher altitude melt-water input from permanent snowfields/glaciers. EC values from November to February (Fig. 4) coincide with a gradual decrease in water level, thus suggesting a decrease in recharge. The undersaturation state of karst springs with respect to calcite and dolomite in most seasons of the year suggests that springs are being fed with an active recharge. The higher partial pressure  $p\text{CO}_2$  for the karst springs than the atmospheric level reveals that springs are not in equilibrium with the atmosphere, maybe due to significant proportions of  $\text{CO}_2$  values from subcutaneous

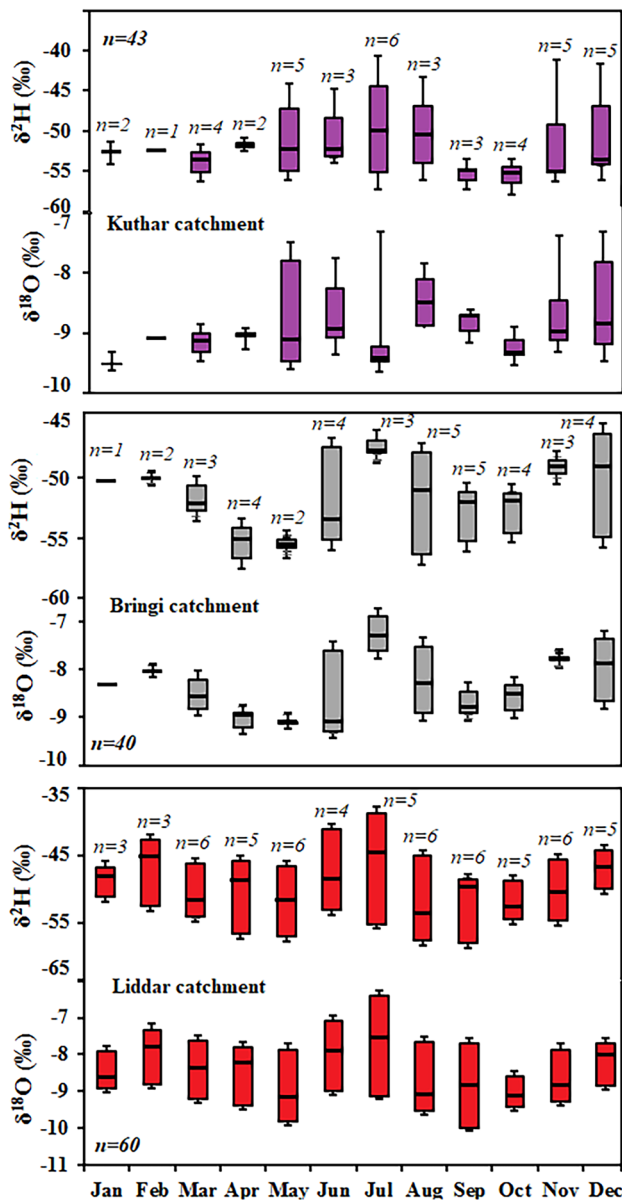


Fig. 5 Spatio-temporal variance in stable water isotopes in karst springs

karstic layers and groundwater in these karstified catchments is aggressive and capable of dissolving the host rock.

**Recharge processes**

Groundwater recharge processes provide first-hand information about the heterogeneity within the aquifer system and the nature of the flow paths with contaminants therein (Jung et al. 2020; Jeelani et al. 2017a; Blasch and Bryson 2007). In the study region, the distinct sinusoidal pattern is seen in the  $\delta$ -values of karst springs can be viewed in context to recharge through differential flow routes and change in

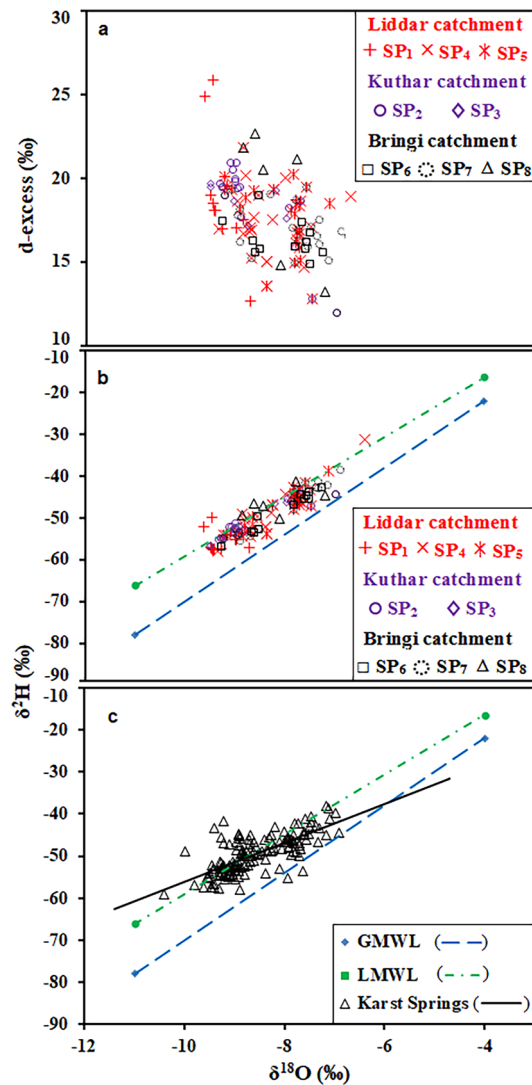
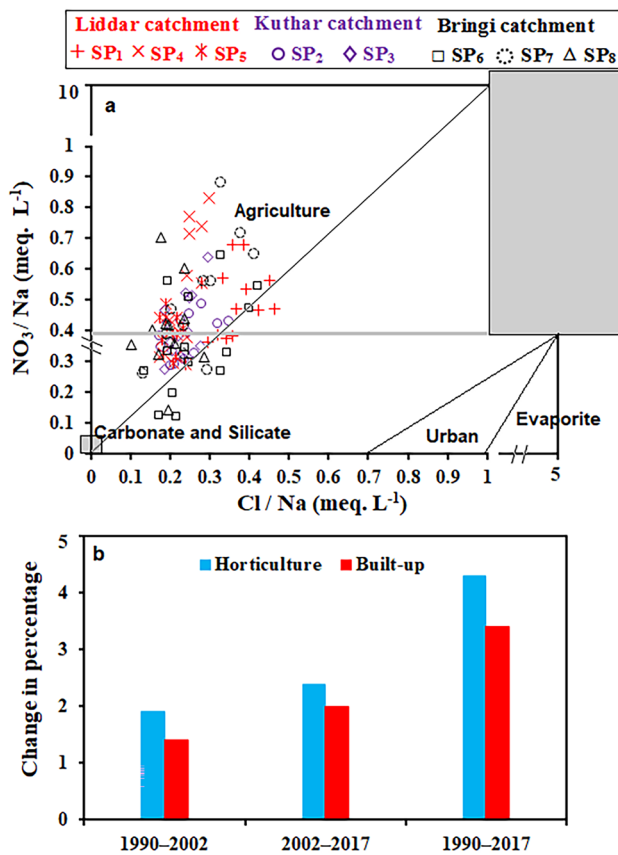


Fig. 6 a D-excess vs  $\delta^{18}O$  of the karst spring, b and c shows the least square regression of  $\delta^2H$  versus  $\delta^{18}O$  of karst springs with respect to the LMWL and GMWL as collective and at catchment scale

seasonal hydro-meteorological conditions at their respective recharge area. The insignificant correlation of the isotopic values of groundwater with altitude may be attributed to different flow paths followed by recharging waters (Jeelani et al. 2017b). Furthermore, in karstified catchments, the heterogeneous secondary permeability can result in a varied hydrographic network (Wang et al. 2020). The temporal pattern seen in  $\delta$ -values of the karst springs indicates the mixing various recharging waters (Solder and Beisner 2020; Joshi et al. 2018). From March to May, the depleted isotopic signal in karst springs is attributed to winter precipitation, released as air temperatures increase (Fig. 5). The rise of the air temperature from March promotes widespread melting of accumulated winter snow, generating higher spring flows with lighter  $\delta$ -values during these months. Meanwhile, the



**Fig. 7** a Scatter plot showing the contribution from anthropogenic forcing and **b** trend analysis of horticulture and built-up from 1990 to 2017

enriched  $\delta$ -values in February, June, and July are attributed to rainfall in these months, with  $\delta$ -values similar to summer rainfall in the recharging altitude. This is because that summer rainfall is distinctly enriched than winter precipitation over the Kashmir Himalayas (Jeelani and Deshpande 2017). The highly depleted yet very little variation in the isotopic signatures (Fig. 5) in the karst springs from August up to the end of October (Fig. 5), when the spring discharge is moderate, are evidence of recharge at higher elevations either from the glaciers and/or permanent snowfields. Since under-zero ambient temperatures occurred in most recharge catchments during the period of low flow between November and January, the stability of isotope values during these periods indicates water is being stored in the aquifer rather than flowing into it.

The lower slopes and lower intercept (collective catchments:  $6.9 (\pm 0.4) \times \delta^{18}\text{O} + 9.8 (\pm 1.4)$ ;  $R^2 = 0.85$ ) of karst springs (Fig. 6c) compared to GMWL and to the established LMWL of Jeelani et al (2017c), reveal evaporation of recharging water before it enters into the aquifer system (Qian et al. 2013, 2014). However, the small difference in slopes and intercepts of the karst springs than LMWL

(Liddar:  $5.8 \pm 0.11$  and  $11 \pm 0.4$ ; Kuthar:  $5.1 \pm 0.21$  and  $7.8 \pm 1.2$ ; Bringi:  $6.3 \pm 0.17$  and  $9.8 \pm 1$ ) in each catchment (Fig. 6b), as well as overlapping/clustering of groundwater samples on LMWL, provides strong evidence of common source recharging waters to karst springs. This similarity is expected in well-karstified carbonate aquifers where high groundwater flow velocity occurs within the high-hydraulic-conductivity solution channels (e.g., flow like underground rivers). Since GMWL (Craig 1961) has a  $d$ -excess of 10‰ which contributes to the formation of meteoric water lines at distinct water vapor sources (Gat 1981). Therefore,  $d$ -excess (or  $d$ ) introduced by Dansgaard (1964) is used as a diagnostic tool to provide accurate information on the amount of moisture/precipitation that has come from different sources to a particular location (Peng et al. 2004; Jeelani and Deshpande 2017), this is because that particular air-sea conditions result in a specific  $d$ -excess value (Gat 1981). Previous studies suggest that precipitation brought by westerly from October to May over the studied region is imprinted with a  $\delta$ -depleted signal associated with higher  $d$  ( $> 16\text{‰}$ ) (Jeelani et al. 2017c; Shah et al. 2017). While the precipitation brought by ISM between June and September months over the region is characterized by the higher  $\delta$ -values with lower  $d$  (Jeelani et al. 2017a; Jeelani and Deshpande 2017). In karst springs, the depleted isotopic fingerprint along with higher  $d$  ( $> 16\text{‰}$ ) (Fig. 6a) is similar to that of winter precipitation across the western Himalayas (e.g. Jeelani et al. 2021, 2018a; b; Lone et al. 2019), which infers winter precipitation (snow) as the predominant source of recharge to the karst springs in the studied catchments. In the winter months, precipitation mainly occurs as snow (Jeelani et al. 2017c), which is stored in snowpacks due to sub-zero temperatures (Jeelani et al. 2013; Shah et al. 2017). Melt-water released from these snowpacks enters the flow system largely from March onward due to increasing temperatures (Jeelani et al. 2018a, b). The reflection of the progressive  $\delta$ -depleted signal and higher  $d$  in karst springs from March to May and from August to October (Figs. 5, 6a) represents the signatures of winter accumulated snow of higher elevations. Moreover, the delayed response of the  $\delta$ -depleted signal of winter precipitation in karst springs also evinces snow as a predominant recharging source to karst springs. Shah et al. (2017) reported that delayed response of  $\delta$ -depleted signal of winter precipitation is characteristic of catchment/region where winter snow significantly contributes to the water resources. Their studies (Jeelani et al. 2013, 2017b) reported that snowmelt sourced from westerly's contributes most to streamflow in studied catchments, making it reasonable to conclude that  $\delta$ -depleted signals associated with higher  $d$  in karst springs reflect depleted winter snow signal. However, the temporal variation in spring flow rates (Fig. 4) results from temporally variable melting processes that govern the isotopic characteristics of karst springs.



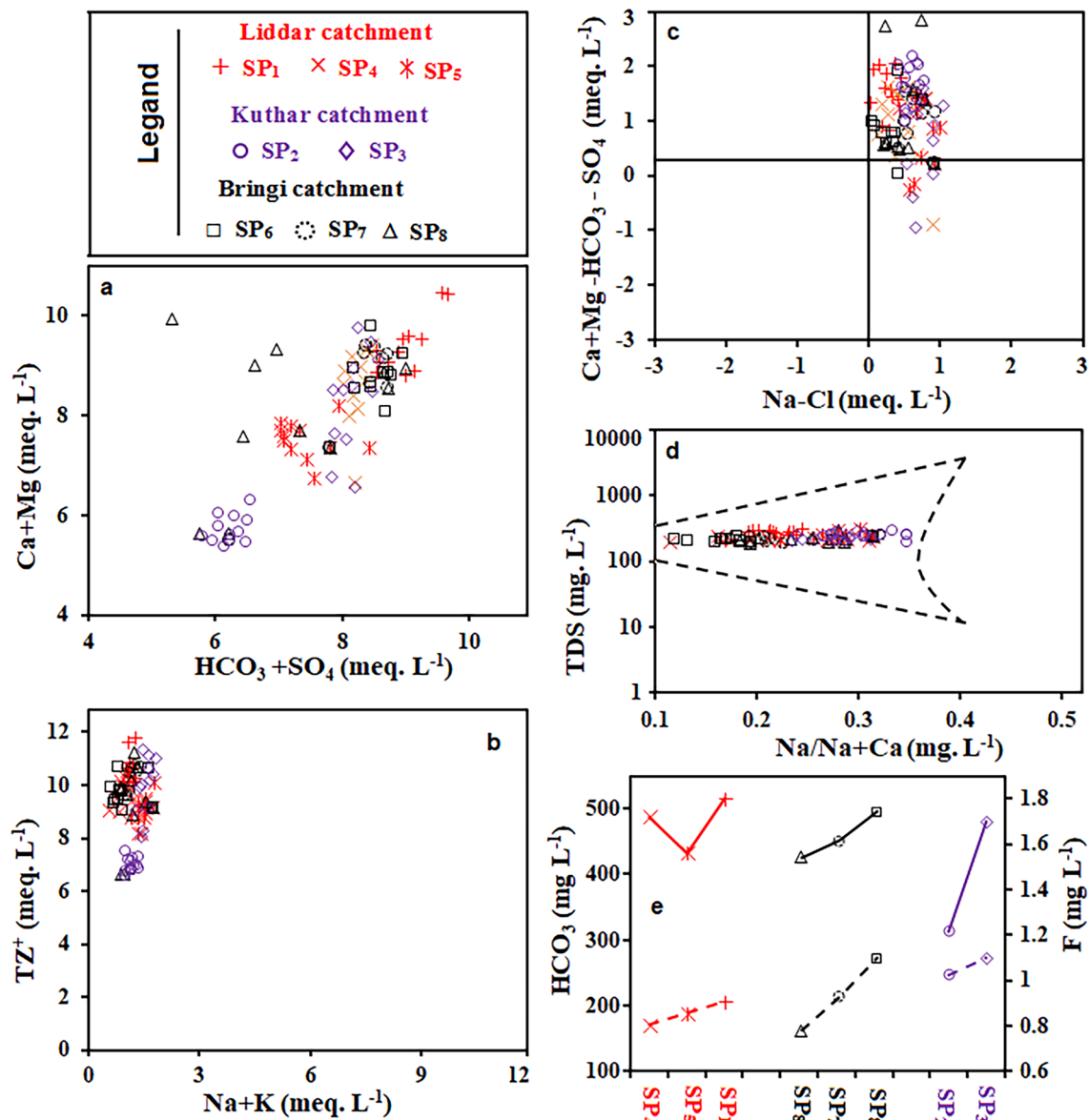


**Fig. 8** Scatter plots of **a**  $\text{Ca}^{2+} + \text{Mg}^{2+}$  versus  $\text{HCO}_3^- + \text{SO}_4^-$ , **b**  $\text{Na}^+ + \text{K}^+$  versus  $\text{TZ}^+$ , **c**  $\text{Ca}^{2+} + \text{Mg}^{2+} - \text{HCO}_3^- - \text{SO}_4^-$  versus  $\text{Na}^+ - \text{Cl}^-$ , and **d**  $\text{Na}/(\text{Na} + \text{Ca})$  versus TDS showing the sources of major

ionic constituents in the karst springs. While sub plot (Fig. 7e) shows the temporal pattern of  $\text{HCO}_3^-$  and  $\text{F}^-$  in the karst springs

Furthermore, it minimizes the effect of enriched signatures of rainfall during the summer and autumn months, except during the significant rain events when  $\delta$ -values are modified and shifted towards heavier isotopic values (e.g., June/July) (refer Fig. 5). These temporal patterns, such as the lagged effects of  $\delta$ -depleted winter precipitation signal and the rapid response of  $\delta$ -enriched spring and summer rainfall events, serve as indicators of hydrologic processes associated with karst aquifers in the studied region. Similarly, the subtle differences in the amplitude of the karst springs suggest different levels of heterogeneity of karst in each catchment. The higher amplitude of karst springs within Bringi,

and Liddar catchments close precipitation coincides with the higher calculated  $k_i$  values (26–59%) (Table 4), suggesting moderately to well-developed karstic aquifers in these catchments. While the lower amplitude (slow response) of springs to recharging events in the Kuthar catchment coincides with lower  $k_i$  values (17–26%), indicating a slight to moderate karstic level. Shah et al (2018), in their study of karst mapping, observed a higher degree of karstification in the Bringi and Liddar catchments and lower in the Kuthar catchment. Considering the above, it can be deduced that in Liddar and Bringi catchments, the preferential flow may occur through conduits network and or/ shorter circuitous

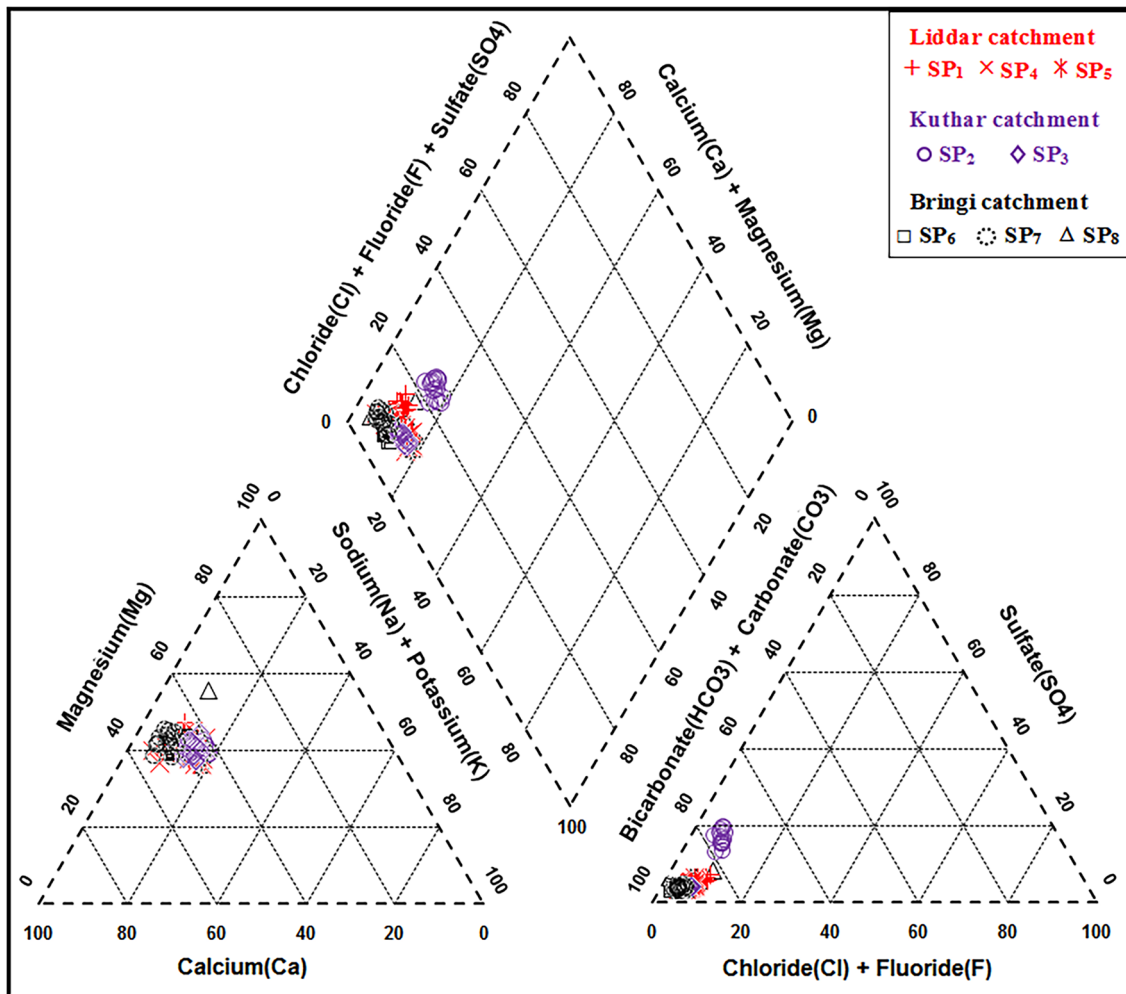


Fig. 9 Piper trilinear plot showing the water types of karst springs in the study region

routes. Wang et al (2020) and Chu et al (2017) explained the rapid response of springs to input signals (higher amplitude close to precipitation) by high aquifer karstification in their studies in karstified catchments in China. However, the longer route at deeper levels of recharging water for springs within the Kuthar catchment can be revealed from their higher water temperatures (17–22 °C) than the spring located in the other two catchments (10–16 °C). Serianz et al. (2020) reported that springs with higher water temperatures (20–23 °C) indicate deep regional flow systems. This coincides with the findings of Shah et al. (2018), who found hypogene (deeper level) karstification in the Kuthar catchment. Since the degree of karstification of an aquifer controls the differences in the hydrogeological function of springs even in similar geological and climatic conditions (Mudarra and Andreo 2011), therefore, the calculated  $ki$  values provide first-hand information on the type of aquifer heterogeneity, which results in varied spring responses to the input signal in the studied region.

## Conclusion

In the present work, karst groundwater which plays a significant role in the water supply and economic development in the entire Kashmir Valley (India), was investigated using ionic constituents and stable water isotopes. The main conclusion is listed below.

1. The study suggested that solute concentrations in spring water are dominantly controlled by the natural mineralization of carbonate and silicate lithologies, which provide insights into preferential groundwater flow in the studied catchments. However, the presence of  $\text{NO}_3^-$ ,  $\text{Cl}^-$ , and  $\text{F}^-$  in the spring waters validates the contribution of anthropogenic forcing within the region.
2. The study found that karst springs are under-saturated with respect to calcite and dolomite and achieve higher partial pressure  $\text{pCO}_2$ , which suggests they are being fed by an active recharge process, and continued dissolu-

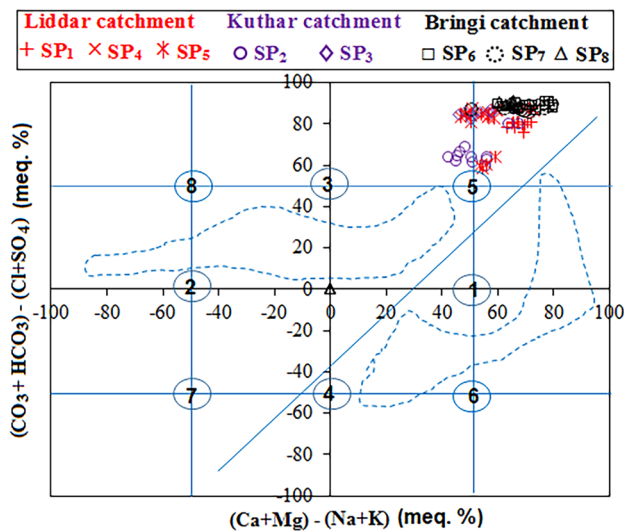


**Fig. 10** Scatter plot showing the hydrogeochemical classification and processes of groundwater in the study region. Each zone illustrates the hydrogeochemical processes as, (1) alkaline earth exceeds alkali metals, (2) alkali metals earth exceeds alkaline earth, (3) weak acidic anions exceeds strong acidic anions, (4) strong acidic anions exceeds weak acidic anions, (5) alkaline earth, and weak acidic anions exceed both alkali metals and strong acidic anions. (6) alkaline earth exceeds alkali metals and strong acidic anions exceed weak acidic anions, (7) alkali earth metals exceed alkaline earth and strong acidic anions exceed weak acidic anions, and (8) alkali metals earth exceeds alkaline earth and weak acidic anions exceed strong acidic anions

tion of the host rocks in most of the seasons. Furthermore, the inverse relationships between discharge and electrical conductivity suggest that new and relatively dilute water is being added to the aquifer in the spring and early summer seasons, which cause strong dilu-

tion effects on the solute concentration of karst springs within the region.

- The study revealed that distinct seasonal patterns in the  $\delta^{18}\text{O}$  and  $\delta^2\text{H}$  of karst springs can be viewed in context to recharge through differential flow routes and changing seasonal hydro-meteorological conditions at their respective recharge area. The depleted isotopic values associated with higher  $d$  ( $> 16\text{‰}$ ) in karst springs suggest that winter precipitation is the primary source of recharge; however, lower values of slope and intercept of spring water regression lines infer evaporation of recharging water before entering the aquifer system.
- The results inferred that lagged effects of  $\delta$ -depleted winter precipitation signal, reflected in spring flow from March to May, and the rapid response of  $\delta$ -enriched spring and summer rainfall events can serve as indicators of hydrologic processes associated with karst aquifers in the studied region.
- Moreover, higher  $k_i$  values and flow-based seasonality of EC and isotopes in karst springs of Liddar and Bringi catchments indicated that groundwater flowed through well-developed drainage systems through large conduits. Conversely, the lower  $ki$  values and higher water temperatures in the Kuthar catchment springs insight hypogene karstification.
- The study recommends that anthropogenic input be restricted in the recharge areas of the karst springs due to the highly karstified nature of the catchments studied. To that end, spreading knowledge about karst landscapes and their resources among the local people will prove effective in protecting the karst aquifers systems within the region.

**Table 4** Parameters used for classifying the karst springs within the study region

Parameter	SP <sub>1</sub>	SP <sub>2</sub>	SP <sub>3</sub>	SP <sub>4</sub>	SP <sub>5</sub>	SP <sub>6</sub>	SP <sub>7</sub>	SP <sub>8</sub>
Spring Flow ( $Q$ ) ( $Q_{min}$ )/( $Q_{max}$ )	0.71	0.36	0.24	0.74	0.35	0.50	0.48	0.66
EC( $Q_{min}$ )/EC( $Q_{max}$ )	1.00	0.95	1.08	1.07	0.99	1.06	0.91	1.08
EC ( $ki$ )	0.72	0.25	0.16	0.58	0.24	0.59	0.43	0.71
Ca <sup>2+</sup> <sub>(Qmin)</sub> /Ca <sup>2+</sup> <sub>(Qmax)</sub>	1.02	1.10	0.99	1.10	0.98	0.93	1.04	0.91
Ca <sup>2+</sup> ( $ki$ )	0.62	0.25	0.20	0.54	0.29	0.51	0.50	0.62
Mg <sup>2+</sup> <sub>(Qmin)</sub> /Mg <sup>2+</sup> <sub>(Qmax)</sub>	0.98	1.05	0.91	0.98	0.99	0.93	0.94	0.86
Mg <sup>2+</sup> ( $ki$ )	0.60	0.22	0.20	0.49	0.27	0.49	0.42	0.59
Na <sup>+</sup> <sub>(Qmin)</sub> /Na <sup>+</sup> <sub>(Qmax)</sub>	0.72	0.67	0.71	0.34	0.60	0.59	0.32	0.50
Na <sup>+</sup> ( $ki$ )	0.51	0.24	0.17	0.25	0.21	0.28	0.11	0.28
K <sup>+</sup> <sub>(Qmin)</sub> /K <sup>+</sup> <sub>(Qmax)</sub>	0.58	0.58	0.36	0.39	0.61	0.50	0.19	0.17
K <sup>+</sup> ( $ki$ )	0.45	0.21	0.09	0.38	0.21	0.27	0.08	0.09
Cl <sup>-</sup> <sub>(Qmin)</sub> /Cl <sup>-</sup> <sub>(Qmax)</sub>	0.97	0.98	0.94	0.93	0.87	1.08	1.05	1.08
Cl <sup>-</sup> ( $ki$ )	0.52	0.29	0.13	0.49	0.22	0.56	0.50	0.73
HCO <sub>3</sub> <sup>-</sup> <sub>(Qmin)</sub> /HCO <sub>3</sub> <sup>-</sup> <sub>(Qmax)</sub>	0.89	0.91	0.87	0.95	0.83	0.94	1.08	0.85
HCO <sub>3</sub> <sup>-</sup> ( $ki$ )	0.63	0.33	0.21	0.70	0.29	0.49	0.43	0.57
SO <sub>4</sub> <sup>-</sup> <sub>(Qmin)</sub> /SO <sub>4</sub> <sup>-</sup> <sub>(Qmax)</sub>	1.04	1.02	1.01	0.90	1.99	1.78	1.19	1.02
SO <sub>4</sub> <sup>-</sup> ( $ki$ )	0.40	0.23	0.16	0.27	0.20	0.88	0.56	0.69
NO <sub>3</sub> <sup>-</sup> <sub>(Qmin)</sub> /NO <sub>3</sub> <sup>-</sup> <sub>(Qmax)</sub>	1.10	0.94	1.43	0.96	1.01	1.19	1.78	1.02
NO <sub>3</sub> <sup>-</sup> ( $ki$ )	0.49	0.20	0.13	0.21	0.19	0.10	0.17	0.12
δ <sup>18</sup> O <sub>(Qmin)</sub> /δ <sup>18</sup> O <sub>(Qmax)</sub>	0.98	0.97	1.07	1.00	1.01	1.20	0.90	0.99
δ <sup>18</sup> O ( $ki$ )	0.93	0.40	0.29	1.03	0.44	0.70	0.52	0.69
ΔCa <sup>2+</sup>	18.1	30.8	11.3	27.4	13.7	45.5	19.1	41
ΔMg <sup>2+</sup>	14.6	23.5	6.2	18.5	11.1	22.1	18	42
ΔNa <sup>+</sup>	7.8	12	8.4	20	14	14	23	17
ΔK <sup>+</sup>	2.2	5.1	4.2	3.8	4.6	5.2	8.3	9.8
ΔCl <sup>-</sup>	8.9	4	9.5	5.6	8.7	10.7	11.8	12
ΔHCO <sub>3</sub> <sup>-</sup>	63	43	42	26	81	185	68.6	229
ΔSO <sub>4</sub> <sup>-</sup>	2.3	6.3	21	4.9	2.2	29.9	7	18
ΔNO <sub>3</sub> <sup>-</sup>	1.2	2.5	2.3	3.3	1.5	4	2.8	4
Karst Index (%)	0.59	0.26	0.17	0.49	0.26	0.49	0.37	0.51
Karst Class	IV	III	II	IV	III	IV	III	IV
Level of Karstification	Well karstified to moderately karstified springs		Slightly karstified spring	Well karstified to moderately karstified Springs				

Note: Δ is the maximum–minimum value of the parameter. Other symbols are discussed in the methods section

**Acknowledgements** The research work was funded by the Department of Science and Technology (DST), Government of India, under the research project DST No: SERB/F/1554/2012. The first author is also thankful to the Director, Wadia Institute of Himalayan Geology (WIHG), Dehradun, India, for the permission to publish this work. The assigned identification number of the manuscript is WIHG/0128.

**Data availability statement** The corresponding authors will be happy to collaborate and share the data with a bonafide researcher upon a reasonable request, which can be sent to the above email address.

**References**

Absar A, Prakash G, Aggarwal RK (1991) A preliminary conceptual model of Nubra Valley Geothermal System, Ladakh, J & K, India. *J Geol Soc India* 37(6):533–545

Atkinson TC (1977) Diffuse flow and conduit flow in limestone terrain in the Mendip Hills, Somerset (Great Britain). *J Hydrol* 35(1–2):93–110. [https://doi.org/10.1016/0022-1694\(77\)90079-8](https://doi.org/10.1016/0022-1694(77)90079-8)

Bakalowicz M (2005) Karst groundwater: a challenge for new resources. *Hydrogeol J* 13:148–160



- Bhat NA, Jeelani G (2015) Delineation of the recharge areas and distinguishing the sources of karst springs in Bringi watershed, Kashmir Himalayas using hydrochemistry and environmental isotopes. *J Earth Sys Sci* 124(8):1667–1676. <https://doi.org/10.1007/s12040-015-0629-y>
- Bhat MI, Zinuddin SM, Rais A (1981) Panjal Trap chemistry and the birth of Tethys. *Geol Mag* 118(4):367–375. <https://doi.org/10.1017/S0016756800032234>
- Blasch KW, Bryson JR (2007) Distinguishing sources of ground water recharge by using  $\delta^2\text{H}$  and  $\delta^{18}\text{O}$ . *Groundwater* 45(3):294–308. <https://doi.org/10.1111/j.1745-6584.2006.00289.x>
- Bonacci O (2015) Surface waters and groundwater in Karst. In: Stevanovic Z (ed) *Karst aquifers—characterization and engineering, professional practice in earth sciences*. Springer Int Pub, Switzerland, vol 5, pp 149–169. [https://doi.org/10.1007/978-3-319-12850-4\\_5](https://doi.org/10.1007/978-3-319-12850-4_5)
- Cattell RB (1966) The scree test for the number of factors. *Multivariate Behav Res* 1(2):245–276. [https://doi.org/10.1207/s15327906mbr0102\\_10](https://doi.org/10.1207/s15327906mbr0102_10)
- Chen Z, Auler AS, Bakalowicz M, Drew D, Griger F, Hartmann J, Jiang G, Moosdorf N, Richts A, Stevanović Z, Veni G, Goldscheider N (2017) The World Karst Aquifer Mapping project: concept, mapping procedure and map of Europe. *Hydrogeol J* 25(3):771–785. <https://doi.org/10.1007/s10040-016-1519-3>
- Chu H, Wei J, Wang R, Xin B (2017) Characterizing the interaction of groundwater and surface water in the karst aquifer of Fangshan, Beijing (China). *Hydrogeol J* 25:575–588. <https://doi.org/10.1007/s10040-016-1507-7>
- Clark I, Fritz P (1997) *Environmental isotopes in hydrogeology*. CRC Press/Lewis Publishers, Boca Raton, New York, p 342. <https://doi.org/10.1002/047147844X.gw211>
- Coplen TB (1995) New manuscript guidelines for the reporting of stable hydrogen, carbon, and oxygen isotope ratio data. *J Petrol* 24(5–6):707–712. <https://doi.org/10.1093/oxfordjournals.petrology.a037273>
- Coward JMH, Waltham AC, Bowser RJ (1972) Karst springs in the Vale of Kashmir. *J Hydrol* 16(3):213–223
- Craig H (1961) Isotopic variation in meteoric waters. *Science* 133:1702–1703. <https://doi.org/10.1126/science.133.3465.1702>
- Dansgaard W (1964) Stable isotopes in precipitation. *Tellus* 16(4):436–468. <https://doi.org/10.1111/j.2153-3490.1964.tb00181.x>
- Dar FA, Perrin J, Riote J, Gebauer HD, Narayana AC, Shakeel A (2011) Karstification in the Cuddapah Sedimentary basin, southern India: implications for groundwater resources. *Acta Carsol* 40(3):457–472. <https://doi.org/10.3986/ac.v40i3.5>
- Dar FA, Perrin J, Narayana AC, Ahmed S (2014a) Review: carbonate aquifers and future perspectives of karst hydrogeology in India. *Hydrogeol J* 22(7):1493–1506
- Dar RA, Romshoo SA, Chandra R, Ahmad I (2014b) Tectono–geomorphic study of the Karewa Basin of Kashmir Valley. *J Asian Earth Sci* 92:143–156. <https://doi.org/10.1016/j.jseaes.2014.06.018>
- Das BK, Kaur P (2001) Major ion chemistry of Renuka lake and weathering processes, Sirmour district, Himachal Pradesh, India. *Env Geol* 40:908–917. <https://doi.org/10.1007/s002540100268>
- Datta NK (1983) Geology, evolution and hydrocarbon prospects of Kashmir Valley. *Pet Asia J* 11:171–179
- Dragon K, Gorski J (2015) Identification of groundwater chemistry origins in a regional aquifer system (Wielkopolska region, Poland). *Environ Earth Sci* 73:2153–2167. <https://doi.org/10.1007/s12665-014-3567-0>
- Dubey DP, Tiwari RN, Dwivedi U (2006) Evaluation of pollution susceptibility of Karst Aquifers of Rewa town (Madhya Pradesh) using “DRASTIC” approach. *J Environ Sci Eng* 48(2):113–118
- Esteller MV, Andreu JM (2005) Anthropogenic effects on hydrochemical characteristics of the Valle de Toluca aquifer (central Mexico). *Hydrogeol J* 13(2):378–390. <https://doi.org/10.1007/s10040-004-0395-4>
- Ford D, Williams P (2007) *Karst hydrogeology and geomorphology*. Wiley, Sussex, pp 1–554
- Frumkin A (2013) New developments of karst geomorphology concepts, editor(s): John F. Shroder. *Treat Geomorphol Acad Press* 6:1–13. <https://doi.org/10.1016/B978-0-12-374739-6.00112-3>
- Fynn OF, Yidana SM, Chegbeleh LP, Yiran GB (2016) Evaluating groundwater recharge processes using stable isotope signatures—the Nabogo catchment of the White Volta, Ghana. *Arab J Geosci* 9(4):279. <https://doi.org/10.1007/s12517-015-2299-0>
- Gat JR (1981) Paleoclimate conditions in the Levant as revealed by the isotopic composition of paleowaters, Israel. *Meteorol Res Paper* 3:13–28
- Ghasemizadeh R, Hellweger F, Butscher C, Padilla I, Vesper D, Field M, Alshawabkeh A (2012) Review: groundwater flow and transport modeling of karst aquifers, with particular reference to the North Coast Limestone aquifer system of Puerto Rico. *Hydrogeol J* 20(8):1441–1461. <https://doi.org/10.1007/s10040-012-0897-4>
- Goldscheider N, Mádl-Szönyi J, Erőss A, Schill E (2010) Thermal water resources in carbonate rock aquifers. *Hydrogeol J* 18:1303–1318. <https://doi.org/10.1007/s10040-010-0611-3>
- Goldscheider N, Chen Z, Auler A, Bakalowicz M, Broda S, Drew D, Hartmann J, Jiang G, Moosdorf N, Stevanovic Z, Veni G (2020) Global distribution of carbonate rocks and karst water resources. *Hydrogeol J* 28:1661–1677. <https://doi.org/10.1007/s10040-020-02139-5>
- Goldscheider N, Drew D (2007) *Methods in Karst hydrogeology*. IAHS Taylor & Francis, London, p 280
- Gunn J (2007) Contributory area definition for groundwater source protection and hazard mitigation in carbonate aquifers. In: Parise M, Gunn J (eds) *Natural and anthropogenic hazards in karst areas: recognition, analysis and mitigation*. Geol Society London, vol 279, pp 97109. <https://doi.org/10.1144/SP279.9>
- Gutiérrez F (2010) Hazards associated with karst. In: Alcántara-Ayala I, Goudie A (eds) *Geomorphological hazards and disaster prevention* (pp 161–176). Cambridge University Press, Cambridge. <https://doi.org/10.1017/CBO9780511807527.013>
- Hartmann A, Goldscheider N, Wagener T, Lange J, Weiler M (2014) Karst water resources in a changing world: review of hydrological modeling approaches. *Rev Geophys* 52:218–242. <https://doi.org/10.1002/2013RG000443>
- He X, Wu J, Guo W (2019) Karst spring protection for the sustainable and healthy living: the examples of Niangziguan spring and Shuishentang spring in Shanxi, China. *Expo Health* 11(2):153–165. <https://doi.org/10.1007/s12403-018-00295-4>
- Heinz B, Birk S, Liedl R, Geyer T, Straub KL, Andresen J, Bester K, Kappler A (2009) Water quality deterioration at a karst spring (Gallusquelle, Germany) due to combined sewer overflow: evidence of bacterial and micro-pollutant contamination. *Environ Geol* 4:797–808
- Jeelani G (2004) Effect of subsurface lithology on hydrochemistry of springs of a part of Kashmir Himalaya. *Himal Geol* 25(2):145–151
- Jeelani G (2005) Chemical quality of the spring waters of Anantnag, Kashmir. *J Geol Soc India* 66(4):453–462
- Jeelani G (2007) Hydrogeology of hard rock aquifer in Kashmir Valley: complexities and uncertainties. In: Ahmed S, Jayakumar R, Salih A (eds) *Groundwater dynamics in hard rock aquifers: sustainable management and optimal monitoring network design*. Capital, New Delhi, pp 243–248
- Jeelani G (2008) Aquifer response to regional climate variability in a part of Kashmir Himalaya in India. *Hydrogeol J* 16:1625–1633. <https://doi.org/10.1007/s10040-008-0335-9>

- Jeelani G (2010) Chemical and microbial contamination of Anantnag springs, Kashmir Valley. *J Himal Ecol Sustain Dev* 5:176–183
- Jeelani G, Deshpande RD (2017) Isotope fingerprinting of precipitation associated with western disturbances and Indian summer monsoons across the Himalayas. *J Earth Syst Sci* 126:108. <https://doi.org/10.1007/s12040-017-0894-z>
- Jeelani G, Bhat NA, Shivanna K (2010) Use of  $\delta^{18}\text{O}$  tracer to identify stream and spring origins of a mountainous catchment: a case study from Liddar watershed, Western Himalaya, India. *J Hydrol* 393(3–4):257–264. <https://doi.org/10.1016/j.jhydrol.2010.08.021>
- Jeelani G, Bhat NA, Shivanna K, Bhat MY (2011) Geochemical characterization of surface water and spring water in SE Kashmir Valley, western Himalaya: implications to water–rock interaction. *J Earth Syst Sci* 120(5):921–932. <https://doi.org/10.1007/s12040-011-0107-0>
- Jeelani G, Kumar US, Kumar B (2013) Variation of  $\delta^{18}\text{O}$  and  $\delta\text{D}$  in precipitation and stream waters across the Kashmir Himalaya (India) to distinguish and estimate the seasonal sources of stream flow. *J Hydrol* 481:157–165
- Jeelani G, Shah RA, Hussain (2014) Hydrogeochemical assessment of groundwater in Kashmir Valley, India. *J Earth Syst Sci* 123(5):1031–1043
- Jeelani G, Shah RA, Deshpande RD, Fryar AE, Perrin J, Mukherjee A (2017a) Distinguishing and estimating recharge to karst springs in snow and glacier dominated mountainous basins of the western Himalaya, India. *J Hydrol* 550:239–252. <https://doi.org/10.1016/j.jhydrol.2017.05.001>
- Jeelani G, Shah RA, Jacob N, Deshpande RD (2017b) Estimation of snow and glacier melt contribution to Liddar stream in a mountainous basin, Western Himalaya: an isotopic approach. *Isotopes Environ Health Stud* 53(1):18–35. <https://doi.org/10.1080/10256016.2016.1186671>
- Jeelani G, Deshpande RD, Shah RA, Hassan W (2017c) Influence of southwest monsoons in the Kashmir Valley, western Himalayas. *Isotopes Environ Health Stud* 53(4):400–412. <https://doi.org/10.1080/10256016.2016.1273224>
- Jeelani G, Shah RA, Fryar AE, Deshpande RD, Mukherjee A, Perrin J (2018a) Hydrological processes in glacierized high-altitude basins of the western Himalayas. *Hydrogeol J* 26(2):615–628. <https://doi.org/10.1007/s10040-017-1666-1>
- Jeelani G, Shah RA, Deshpande RD (2018b) Assessment of Groundwater in Karst System of Kashmir Himalayas, India. In: Mukherjee A (eds) *Groundwater of South Asia*. Springer Nature, Singapore, pp 85–100. [https://doi.org/10.1007/978-981-10-3889-1\\_6](https://doi.org/10.1007/978-981-10-3889-1_6)
- Jeelani G, Shah RA, Deshpande RD, Dimri AP, Mal S, Sharma A (2021) Isotopic analysis to quantify the role of the Indian monsoon on water resources of selected river basins in the Himalayas. *Hydrol Proces* 35(11):14406
- Joshi K, Rai SP, Sinha R, Gupta S, Densmore AL, Rawat YS, Shekhar S (2018) Tracing groundwater recharge sources in the northwestern Indian alluvial aquifer using water isotopes ( $\delta^{18}\text{O}$ ,  $\delta^2\text{H}$  and  $^3\text{H}$ ). *J Hydrol* 559:835–847. <https://doi.org/10.1016/j.jhydrol.2018.02.056>
- Jung H, Koh DC, Kim YS, Jeon SW, Lee J (2020) Stable isotopes of water and nitrate for the identification of groundwater flowpaths: a review. *Water* 12(1):138. <https://doi.org/10.3390/w12010138>
- Kaiser HF (1960) The application of electronic computers to factor analysis. *Educ Psychol Meas* 20(1):141–151
- Katz BG, Coplen TB, Bullen TD, Davis JH (1997) Use of chemical and isotopic tracers and geochemical modeling to characterize the interactions between ground water and surface water in mantled karst. *Groundwater* 35(6):1014–1028. <https://doi.org/10.1111/j.1745-6584.1997.tb00174.x>
- Kou Y, Li Z, Hua K, Li Z (2019) Hydrochemical characteristics, controlling factors, and solute sources of streamflow and groundwater in the Hei River catchment, China. *Water* 11(11):2293. <https://doi.org/10.3390/w11112293>
- Lee SK, Nam KA, Hoe YH, Min HY, Kim EY, Ko H, Kim S et al (2003) Synthesis and evaluation of cytotoxicity of stilbene analogues. *Arch Pharm Res* 26(4):253–257. <https://doi.org/10.1007/bf02976951>
- Li P, Zhang Y, Yang N, Jing L, Yu P (2016) Major ion chemistry and quality assessment of groundwater in and around a mountainous tourist town of China. *Expo Health* 8(2):239–252. <https://doi.org/10.1007/s12403-016-0198-6>
- Li P, Wu J, Tian R, He S, He X, Xue C, Zhang K (2018) Geochemistry, hydraulic connectivity and quality appraisal of multilayered groundwater in the Hongdunzi Coal Mine, northwest China. *Mine Water Environ* 37(2):222–237. <https://doi.org/10.1007/s10230-017-0507-8>
- Li P, Tian R, Liu R (2019) Solute geochemistry and multivariate analysis of water quality in the Guohua Phosphorite Mine, Guizhou Province, China. *Expo Health* 11(2):81–94. <https://doi.org/10.1007/s12403-018-0277-y>
- Liu T, Gao X, Zhang X, Li C (2020) Distribution and assessment of hydrogeochemical processes of F-rich groundwater using PCA model: a case study in the Yuncheng Basin, China. *Acta Geochim* 39(2):216–225. <https://doi.org/10.1007/s11631-019-00374-6>
- Lone S, Jeelani G, Deshpande RD, Mukherjee A (2019) Stable isotope ( $\delta^{18}\text{O}$  and  $\delta\text{D}$ ) dynamics of precipitation in a high altitude Himalayan cold desert and its surroundings in Indus river basin, Ladakh. *Atmos Res* 221:46–57. <https://doi.org/10.1016/j.atmosres.2019.01.025>
- López-Chicano M, Bouamama M, Vallejos A, Pulido-Bosch A (2001) Factors which determine the hydrogeochemical behaviour of karstic springs. A case study from the Betic Cordilleras, Spain. *Appl Geochem* 16(9–10):1179–1192. [https://doi.org/10.1016/S0883-2927\(01\)00012-9](https://doi.org/10.1016/S0883-2927(01)00012-9)
- Maurya AS, Shah M, Deshpande RD, Gupta SK (2009) Protocol for  $\delta^{18}\text{O}$  and  $\delta\text{D}$  analyses of water sample using Delta V plus IRMS in CF mode with gas bench II for IWIN National Programme at PRL, Ahmedabad. In: 11th ISMAS Triennial Conference of Indian Society for Mass Spectrometry (vol 314, pp 314–317). Indian Society for Mass Spectrometry Hyderabad
- McGuire KJ, DeWalle DR, Gburek WJ (2002) Evaluation of mean residence time in subsurface waters using oxygen-18 fluctuations during drought conditions in the mid Appalachians. *J Hydrol* 261:132–149. [https://doi.org/10.1016/S0022-1694\(02\)00006-9](https://doi.org/10.1016/S0022-1694(02)00006-9)
- Middlemiss CS (1910) Revision of Silurian-Triassic sequence of Kashmir. *Rec Geol Surv India* 40(3):206–260
- Mudarra M, Andreo B (2011) Relative importance of the saturated and the unsaturated zones in the hydrogeological functioning of karst aquifers: the case of alta cadena (southern Spain). *J Hydrol* 397:263–280. <https://doi.org/10.1016/j.jhydrol.2010.12.005>
- Mustafa O, Merkel B (2015) Classification of karst springs based on discharge and water chemistry in Makook karst system, Kurdistan Region, Iraq. *Freiberg Online Geosci* 39:1–24
- Nesrine N, Rachida B, Ahmed R (2015) Multivariate statistical analysis of saline water—a case study: sabkha Oum LeKhialate (Tunisia). *Int J Environ Sci Dev* 6(1):40. <https://doi.org/10.7763/IJESD.2015.V6.558>
- Ophori DU, Toth J (1989) Characterization of groundwater flow by field mapping and numerical simulation, Ross Creek Basin, Alberta, Canada. *Groundwater* 27(2):193–201. <https://doi.org/10.1111/j.1745-6584.1989.tb00440.x>
- Parise M (2016) How confident are we about the definition of boundaries in karst? Difficulties in managing and planning in a typical transboundary environment. In: Stevanovic Z, Kresic N, Kukuric N (eds) *Karst without boundaries*. CRC Press, Boca Raton, vol 23, pp 27–38. <https://doi.org/10.1201/b21380-4>

- Parise M, Gabrovsek F, Ravbar N (2018) Recent advances in karst research: from theory to fieldwork and applications. *Geol Soc Lond Spec Pub* 466:124. <https://doi.org/10.1144/SP466.26>
- Parkhurst DL, Appelo CA (2013) Description of input and examples for PHREEQC (Version 3)-a computer program for speciation, batch-reaction, one-dimensional transport, and inverse geochemical calculations. In: Chapter 43 of section A, *Groundwater Books, Modelling Techniques*. <https://pubs.usgs.gov/tm/06/a43>
- Peng H, Mayer B, Harris S, Krouse HR (2004) A 10-year record of stable isotope ratios of hydrogen and oxygen in precipitation at Calgary, Alberta, Canada. *Tellus B* 56:147–159. <https://doi.org/10.3402/tellusb.v56i2.16410>
- Perrin J, Pochon A, Jeannin PY, Zwahlen F (2004) Vulnerability assessment in karstic areas: validation by field experiments. *Environ Geol* 46:237–245. <https://doi.org/10.1007/s00254-004-0986-3>
- Price RM, Swart PK, Willoughby HE (2008) Seasonal and spatial variation in the stable isotopic composition of  $\delta^{18}\text{O}$  and  $\delta\text{D}$  of precipitation in south Florida. *J Hydrol* 358:193–205. <https://doi.org/10.1016/j.jhydrol.2008.06.003>
- Qian H, Li P, Wu J, Zhou Y (2013) Isotopic characteristics of precipitation, surface and ground waters in the Yinchuan Plain, northwest China. *Environ Earth Sci* 70(1):57–70. <https://doi.org/10.1007/s12665-012-2103-3>
- Qian H, Wu J, Zhou Y, Li P (2014) Stable oxygen and hydrogen isotopes as indicators of lake water recharge and evaporation in the lakes of the Yinchuan Plain. *Hydrol Process* 28:3554–3562. <https://doi.org/10.1002/hyp.9915>
- Rashrash S, Ghawar B, Hweesh A (2015) Evaluating groundwater pollution using hydrochemical data: case study (Al Wahat Area East of Libya). *J Wat Resour Protect* 7:369–377. <https://doi.org/10.4236/jwarp.2015.74029>
- Rao NS, Rao JP, Subrahmanyam A (2007) Principal component analysis in groundwater quality in a developing urban area of Andhra Pradesh. *J Geol Soc India* 69(5):959–969
- Rasool R, Fayaz A, Shafiq M, Singh H, Ahmed P (2021) Land use land cover change in Kashmir Himalaya: linking remote sensing with an indicator based DPSIR approach. *Ecol Indic* 125:107447. <https://doi.org/10.1016/j.ecolind.2021.107447>
- Ren X, Li P, He X, Su F, Elumalai V (2021) Hydrogeochemical processes affecting groundwater chemistry in the central part of the Guanzhong Basin, China. *Arch Environ Contam Toxicol* 80(1):74–91. <https://doi.org/10.1007/s00244-020-00772-5>
- Savio D, Stadler P, Reischer GH, Demeter K, Linke RB, Blaschke AP, Mach RL, Kirschner AKT, Stadler H, Farnleitner AH (2019) Spring water of an alpine karst aquifer is dominated by a taxonomically stable but discharge-responsive bacterial community. *Front Microbiol* 10:28. <https://doi.org/10.3389/fmicb.2019.00028>
- Serianz L, Rman N, Brencic M (2020) Hydrogeochemical characterization of a warm spring system in a carbonate mountain range of the Eastern Julian Alps. *Slovenia Water* 12:1427. <https://doi.org/10.3390/w12051427>
- Shah RA, Jeelani G (2016) Vulnerability of karst aquifer to contamination: a case study of Liddar catchment, Kashmir Himalayas. *J Himal Ecol Sustain Dev* 11:58–72
- Shah RA, Jeelani G, Jacob N (2017) Estimating mean residence time of karst groundwater in mountainous catchments of Western Himalaya, India. *Hydrol Sci J* 62(8):1230–1242. <https://doi.org/10.1080/02626667.2017.1313420>
- Shah RA, Jeelani G, Goldscheider N (2018) Karst geomorphology, cave development and hydrogeology in the Kashmir valley, Western Himalaya, India. *Acta Carsol* 47(1):5–21. <https://doi.org/10.3986/ac.v47i1.5178>
- Shibasaki T, Balakrishna S, Yoshimura T, Venkatanarayana B, Furu-kama H, Venkateswara RT, Chuman N, Ramanohan RY, Venkateswala K (1985) Karstification process of carbonate rocks in the Cuddapah sedimentary Basin, Indian Peninsular Shield. *J Fac Mar Sci Technol Tokai Univ* 21:31–45
- Singh Y (1985) Hydrogeology of the karstic area around Rewa, MP, India. In: *Karst water resources, Proc. of the Ankara-Antalya Symposium*. IAHS Publ. No. 161, IAHS, Wallingford, UK
- Singh Y, Dubey DP (1997) Deep zone karst aquifers as a boon in central India. In: Beck BF, Stephenson JB (eds) *The Engineering geology and hydrogeology of Karst Terranes*. A. A. Balkema Publisher, Rotterdam, pp 245–249
- Solder JE, Beisner KR (2020) Critical evaluation of stable isotope mixing end-members for estimating groundwater recharge sources: case study from the South Rim of the Grand Canyon, Arizona, USA. *Hydrogeol J* 28:1575–1591. <https://doi.org/10.1007/s10040-020-02194-y>
- Stevanović Z (2019) Karst waters in potable water supply: a global scale overview. *Environ Earth Sci* 78:662. <https://doi.org/10.1007/s12665-019-8670-9>
- Szramek K, Walter LM, Kanduč T, Ogrinc N (2011) Dolomite versus Calcite weathering in hydrogeochemically diverse watersheds established on bedded carbonates (Sava and Soča Rivers, Slovenia). *Aquat Geochem* 17(4–5):357–396
- Tang C, Jin H, Liang Y (2021) Using isotopic and hydrochemical indicators to identify sources of sulfate in Karst groundwater of the Niangziguan Spring Field, China. *Water* 13:390. <https://doi.org/10.3390/w13030390>
- Vesper DJ, White WB (2003) Metal transport to karst springs during storm flow: an example from Fort Campbell, Kentucky/Tennessee, USA. *J Hydrol* 276:20–36. [https://doi.org/10.1016/S0022-1694\(03\)00023-4](https://doi.org/10.1016/S0022-1694(03)00023-4)
- Vinnarasi F, Srinivasamoorthy K, Saravanan K, Gopinath S, Prakash R, Ponnunani G, Babu C (2021) Chemical weathering and atmospheric carbon dioxide ( $\text{CO}_2$ ) consumption in Shanmuganadhi, South India: evidences from groundwater geochemistry. *Environ Geochem Health* 43(2):771–790. <https://doi.org/10.1007/s10653-020-00540-3>
- Vogelbacher A, Kazakis N, Voudouris K, Bold S (2019) Groundwater vulnerability and risk assessment in A Karst Aquifer of Greece using EPIK Method. *Environ* 6:116. <https://doi.org/10.3390/envir0nments6110116>
- Vreča P, Kern Z (2020) Use of water isotopes in hydrological processes. *Water* 12(8):2227. <https://doi.org/10.3390/w12082227>
- Wadia DN (1975) *Geology of India*. Tata McGraw Hill Co, New Delhi, p 344
- Waltham AC (1972) Caving in the Himalaya. *Himal J* 31:9. <http://www.himalayanclub.org/hj/31/9/caving-in-the-himalaya>
- Wang F, Chen H, Lian J, Fu Z, Nie Y (2020) Seasonal recharge of spring and stream waters in a Karst catchment revealed by isotopic and hydrochemical analyses. *J Hydrol*. <https://doi.org/10.1016/j.jhydrol.2020.125595>
- Wei M, Wu J, Li W, Zhang Q, Su F, Wang Y (2021) Groundwater geochemistry and its impacts on groundwater arsenic enrichment, variation, and health risks in Yongning County, Yinchuan Plain of northwest China. *Expo Health*. <https://doi.org/10.1007/s12403-021-00391>
- Wu J, Li P, Qian H, Duan Z, Zhang X (2014) Using correlation and multivariate statistical analysis to identify hydrogeochemical processes affecting the major ion chemistry of waters: case study in Laoheba phosphorite mine in Sichuan, China. *Arab J Geosci* 7(10):3973–3982. <https://doi.org/10.1007/s12517-013-1057-4>
- Wu J, Li P, Wang D, Ren X, Wei M (2020) Statistical and multivariate statistical techniques to trace the sources and affecting factors of groundwater pollution in a rapidly growing city on the Chinese Loess Plateau. *Hum Ecol Risk Assess* 26(6):1603–1621. <https://doi.org/10.1080/10807039.2019.1594156>

- Younos T, Schreiber M, Kosič Ficco K (2019) Karst water environment: advances in research, management and policy. Springer Cham. <https://doi.org/10.1007/978-3-319-77368-1>
- Yu S, Chae G, Oh J, Kim SH, Kim D, Yun ST (2021) Hydrochemical and isotopic difference of spring water depending on flow type in a stratigraphically complex karst area of South Korea. *Front Ear Sci* 9
- Zakhem AB, Charideh A, Kattaa B (2017) Using principal component analysis in the investigation of groundwater hydrochemistry of Upper Jezireh Basin, Syria. *Hydrol Sci J* 62(14):2266–2279. <https://doi.org/10.1080/02626667.2017.1364845>
- Zhao S, Hu H, Tian F, Tie Q, Wang L, Liu Y, Shi C (2017) Divergence of stable isotopes in tap water across China. *Sci Rep* 7:43653. <https://doi.org/10.1038/srep43653>

**Publisher's Note** Springer Nature remains neutral with regard to jurisdictional claims in published maps and institutional affiliations.